Atmos. Chem. Phys. Discuss., 10, 20461–20514, 2010
www.atmos-chem-phys-discuss.net/10/20461/2010/
doi:10.5194/acpd-10-20461-2010

Atmospheric Chemistry and Physics Discussions

Investigating the sensitivity of high-resolution mesoscale models to microphysical parameters by the use of polarimetric radar observations

R. Ferretti[1], **K. De Sanctis**[1,*], **L. Molini**[2], **A. Parodi**[2], **M. Montopoli**[1,3], **F. S. Marzano**[1,4], **and F. Siccardi**[2,5]

[1]CETEMPS – Department of Physics, University of L'Aquila, L'Aquila, Italy
[2]CIMA Research Foundation, University Campus, Savona, Italy
[3]DIEI, University of L'Aquila, L'Aquila, Italy
[4]DIE, Sapienza University of Rome, Rome, Italy
[5]DIST, University of Genoa, Genoa, Italy
[*]now at: HIMET s.r.l, L'Aquila, Italy

Received: 18 June 2010 – Accepted: 20 July 2010 – Published: 27 August 2010

Correspondence to: R. Ferretti (rossella.ferretti@aquila.infn.it)

Published by Copernicus Publications on behalf of the European Geosciences Union.

Abstract

An improved methodology for investigating mesoscale model microphysics is presented and discussed for a case study. Polarimetric radar data are used to assess numerical weather prediction (NWP) model's skill in reproducing the microphysical features of severe rainfall. To this aim, an event of deep convection, developed on 20 May 2003 in the Po Valley (Italy), is analyzed. During the selected case study, two weather radars, sited in Gattatico and San Pietro Capofiume (near Bologna, Italy), detected a deep-convective and hail cell with a large inner graupel core which reached the ground, as was reported by local weather authorities and citizens. A hydrometeor classification algorithm, based on a Bayesian approach and a radar simulator model, are used to retrieve the vertical structure of the storm and characterize its ground effects. These products are used for evaluating the sensitivity of NWP models with respect to the graupel density, described in terms of the intercept parameter of the graupel size distribution and its depositional velocity. To this purpose two mesoscale NWP models, specifically COSMO-LAMI and MM5-V3, are used at high spatial resolution. Their ability in reproducing the vertical and the horizontal structure and the microphysical distribution of the major convective cell is evaluated. Both models show large sensitivity to different microphysical settings and a capability to reproduce fairly well the observed hail cell. Ground-radar reflectivity fields and the hydrometeor vertical structure are correctly simulated by both NWP models as opposed to a failure in reproducing the graupel distribution near the ground.

1 Introduction

The predictability of an extreme hydro-meteorological event requires the combined analysis of forecasts provided by Numerical Weather Prediction (NWP) models and observations (e.g., rain gauges and remote sensors). The merging of modeling and observational data is a complex task, since such events are often convective in nature

ACPD
10, 20461–20514, 2010

and characterized by small spatial-temporal scales. Radar simulator models have been used to compare NWP model results and observations since the early 1970s (e.g., Smith et al., 1975, and many others). Recently, NWP models and observational tools largely improved: NWP reached a spatial resolution of a few kilometers, explicitly solving convection and partly the inner cloud structure, whilst precipitation retrievals by either space-born and/or ground-based weather radars allowed to improve the initial condition reliability and provided a robust forecast verification framework.

In the past years the scientific community recognized the key role of the microphysical parameterization in the high-resolution NWP models and its capability in reproducing the cloud structure became a challenging task. Typically, the microphysical particle size distribution (PSD) has been represented by one-moment bulk parameterization within NWP models; recent developments have led to different approaches: 1) higher order parameterizations, i.e. the two-moment scheme (Morrison et al., 2005); 2) bin or spectral schemes (Lynn et al., 2005a,b); 3) improvements in the one-moment bulk parameterization by a more consistent representation of cloud processes. Furthermore, understanding the role of uncertainties inherent the cloud-scale microphysical parameterizations is one important issue of deep convection dynamics (Droegemeier et al., 2000).

Few years ago, the Improvement of Microphysical Parameterization through Observational Verification Experiment (IMPROVE) campaign was held over the Oregon Cascade Mountains in order to collect measurements of cloud microphysical variables useful to improve the bulk microphysical parameterizations into mesoscale models (Stoelinga et al., 2003). During the campaign several events were observed and the measured snow PSD allowed assessing the major role of the snow intercept parameter and of its total mass concentration in correctly modeling the precipitation. Garvert et al. (2005) found that an overestimation of the mass concentration of snow aloft produced an overestimation of the precipitation on the lee side of the Oregon Cascade. Gilmore et al. (2004) studied the microphysics uncertainty due to variations in size-related precipitation particle parameters and showed convection properties at storm

ACPD
10, 20461–20514, 2010

scale to be very sensitive to changes in the intercept parameter, for rain, snow and graupel. They also showed that the amount of accumulated precipitation at the ground was depending on graupel/hail category parameterization schemes. In addition, they argued that particle size distributions, characterized by larger intercepts and/or smaller particle density, had a smaller mass-weighted mean terminal fall velocity and produced smaller hail mixing ratios spread over a larger area. Once more, Gilmore et al. (2004) noted that the inclusion of a fast-falling graupel/hail species resulted in an enhanced low-level cloud precipitating water and greater accumulated precipitation produced by simulated supercell and multicell storms. They also found that the distribution of hydrometeor species changed dramatically aloft as the intercept parameter for graupel/hail was changed. Van den Heveer and Cotton (2004) assessed the impact of hail size distribution on simulated supercell storms using the Regional Atmospheric Modeling System (RAMS): they showed that increasing the mean hail equivalent diameter led to an increase in the mean terminal fall speed of the hail species and to reduced melting and evaporation rates. Their numerical sensitivity experiments demonstrated that the low-level downdrafts were stronger, the cold pools were deeper and more intense and the low-level vertical vorticity was greater in cases studies where smaller hail stones were simulated.

The spatial-temporal properties of deep convective processes were analyzed by several other studies (Cotton et al., 1982; McCumber et al., 1991; Ferrier et al., 1995; Proctor, 1988, 1989; Straka and Anderson, 1993; Cohen and McCaul, 2006) showing that the characteristics of the different ice hydrometeors used in convection-resolving simulations of thunderstorms greatly influence the precipitation distribution. Recently, Tong and Xue (2008) investigated the possibility of estimating fundamental parameters common to many single-moment ice schemes using radar observations for a model-simulated supercell storm by performing a parameter sensitivity analysis. They considered the PSD intercept parameters for rain, snow and hail/graupel, and the bulk densities of snow and hail/graupel; their results suggested that the errors in the microphysical parameters had a larger impact on model microphysical fields than on wind

ACPD
10, 20461–20514, 2010

fields. Finally, May et al. (2007) showed the use of a Doppler radar emulator based on Raylegh scattering to evaluate the circulation associated with a tornado within a supercell thunderstorm, simulated by the Advanced Regional Prediction System (ARPS). In their work several metrics for tornado intensity were examined to assess the degradation of the tornadic signature as a function of range and azimuthal sampling intervals.

Following Gilmore et al. (2004), Reinhardt and Seifert (2006) carried out sensitivity tests to microphysics for the COSMO local area model (LAM), finding a general agreement with Gilmore's numerical experiments: setting graupel/hail weighted toward large hail generally produced an increase of ground precipitation. The sensitivity of the Mesoscale Model 5 (MM5) model to microphysical parameters was also investigated by Serafin and Ferretti (2007) by using three different bulk microphysical parameterization schemes for two cases, respectively, of heavy and light precipitation in the Po Valley. They compared the simulated vertical profiles of hydrometeors with available radar observations showing gross similarities for two of the analyzed schemes. Moreover, they also investigated the role of the snow fall speed. The results suggested that these parameters did not seem to largely influence MM5's forecast skill systematically; the impact of changes in the parameterization of the snow deposition velocity very likely depended on the dynamics of the event under investigation.

According to the aforementioned studies, a matrix design of LAM numerical simulations, similar to that used by Gilmore et al. (2004) and by Reinhardt and Seifert (2006), has been performed in this paper to assess the microphysical sensitivity of the NWP model themselves. An extensive methodology to investigate the cloud-scale microphysics performance is addressed. The latter includes the use of two different local area models, i.e., MM5 version-3 (MM5-V3) and COSMO LAM Italy (COSMO-LAMI), coupled with a weather radar simulator and an advanced radar-based hydrometeor classification technique. This approach allows to compare LAM numerical prediction outputs with weather radar observations directly in terms of microphysical species. The Bayesian Radar Algorithm for Hydrometeor Classification at C-band (BRAHCC, detailed in Marzano et al., 2008), has been here implemented for this purpose. Clas-

ACPD
10, 20461–20514, 2010

sification procedures aim to provide a class code which is not easy to compare with in situ data or other sources. A more natural product of an overall hydrometeor retrieval algorithm may be the estimation of the hydrometeor water content (e.g., Marzano et al., 1999, 2008) since it may simplify both the comparison with models and the radar data assimilation within NWP models. Within this methodological framework, it can be directly evaluated which microphysics setting gives the closest simulation to the observations.

A further intercomparison model-observation approach is envisaged by applying a polarimetric radar simulator model (RSM-POL) to LAM outputs too. Haase and Crewell (2000) paper clearly showed how the basic reflectivity equation was applied in conjunction with a T-matrix approach and the associated attenuation effects. Based on this work, Molini et al. (2008) added the differential reflectivity to the basic components of the Haase and Crewell radar simulator, showing the sensitivity of simulated-radar-retrieved variables (using the classification algorithm of Straka et al., 2000) to the attenuation the simulated radar beam undergoes. To the authors knowledge this is the first study aimed to perform comparisons using BRAHCC and RSM-POL methodology and a suite of sensitivity runs for a convective case in the Po Valley (Italy).

Therefore, the major issues, this work deals with, are: i) performing hydrometeor classification retrieval (for both precipitation type and amount) applied to observed/modeled radar data; ii) assessing the sensitivity of the models to changes on their graupel microphysical configurations; iii) establishing the best NWP mesoscale model configuration by weather radar observations. A case study of hailstorm already observationally investigated by Marzano et al. (2007, 2008) is chosen for this paper. On 20 May 2003 a hailstorm occurred in the flat lands of North-Eastern Italy; this event was monitored by two polarimetric C-band radars located 90 km apart in the Po Valley of Northern Italy, one in S. Pietro Capofiume (SPC hereafter) and the other in Gattatico (GAT hereafter). Due to the hailstorm nature of this event, the sensitivity to graupel particle properties (density, number density intercept, velocity/size and mass/size distribution) are investigated at high resolution (1 km) using two mesoscale models. For

ACPD
10, 20461–20514, 2010

this purpose several microphysical settings, going from light and slowly falling graupel to medium/heavy and fast falling hail, are considered. The different settings are analyzed in terms of correct location/misplacement of the cell produced by the models, reflectivity maps and vertical cross section of reflectivity. The mean vertical columnar contents are also analyzed, together with the hydrometeors classification, both for a vertical cross section and the horizontal distribution. Finally, a spectral analysis is performed to quantify the LAMs response to the different hydrometeors in order to statistically assess the spatial-temporal models deviations from a statistical standpoint.

The paper has been organized as follows. Section 2 presents the hailstorm event, whereas Sect. 3 presents the available radar observations, the microphysical radar retrieval algorithm and finally a radar simulator model used in the paper. In Sect. 4 the non-hydrostatic models COSMO-LAMI and MM5-V3 are described. Section 5 is devoted to an accurate discussion of the sensitivity analysis and of the performed numerical experiments. Section 6 presents and discusses the results of the numerical experiments for COSMO-LAMI and MM5-V3 and their comparison with radar observations, in terms of reflectivity and microphysical retrieved fields. In Sect. 7 conclusions are drawn.

2 Case study

The event chosen for this study is characterized by an upper level trough sweeping northern Italy from North West and a relatively weak low level depression on 20 May 2003 at 00:00 UTC (Fig. 1). The low level depression slightly deepens by 12:00 UTC on 20 May (Fig. 1c), allowing a cyclonic circulation to develop on the northern Italy plains, which advects humid air toward the area under consideration (Fig. 1c). This structure lasts until early afternoon of 20 May. The north eastern flank of the cyclonic circulation produces a northeastern wind (Figs. 1d and 2d) on the east side of the north Italy plains, largely destabilizing the atmosphere because of the cold dry air intrusion. Initially, an intense westerly flow is detected at middle-upper levels associated with

ACPD
10, 20461–20514, 2010

a variable wind at lower level. A strong vertical wind shear is observed until 00:00 UTC 20 May (Fig. 2a); in the following hours wind intensifies also at lower level and it turns into southwesterly at 06:00 UTC 20 May (Fig. 2b). In particular, the vertical wind profile shows a remarkable positive velocity shear between mean and high troposphere since a moderately powerful jet stream (80 knots from SSW) at 250 hPa and a 37-knot equally-oriented current at 500 hPa are observed by the 12:00 UTC Udine sounding (Fig. 2c).

Such a shear condition easily succeeds in promoting and feeding relevant hail-producing updrafts, once convection is started by frontal system or other local mechanisms. The cold dry air intrusion, which is also associated with dry air entering from west (following the trough) clearly visible from the satellite imagery (Fig. 3, dark tongue), produces the suitable environment for the vertical development of deep convection by middle day (Fig. 3). Hail is detected by both SPC and GAT weather radars during the afternoon. This point will be further discussed in the next section.

3 C-band weather radar data

Reflectivity data have been provided by the C-band operational Doppler radars of SPC and GAT, located in the Po Valley in northern Italy.

Both of them are dual-polarization radars, placed on a tower with a Cassegrain parabolic antenna (without radome cover), providing a half-power beam-width of 1.0° and a directivity of about 45-dB. The klystron peak-power is 250 kW at 5.6 GHz with an alternating horizontal-vertical polarization transmission and a dual pulse repetition frequency (PRF) system for unfolding capability. Pulse widths of 0.5 ms (i.e., short pulse with a re-sampled bin resolution of 250 m) and 1.5 ms (i.e., long pulse with a re-sampled bin resolution of 1500 m) are used. The receiver sensitivity is equal to 113 dBm. The typically used maximum range is 250 km (with long pulse) and 125 km (with short pulse), respectively, for the intensity and velocity mode.

ACPD
10, 20461–20514, 2010

Radar data are acquired with a prescribed scanning strategy during operational activities, consisting of 15 elevations with an angular spacing of 1.0°. Radial spatial resolution is set to 250 m for short ranges (i.e., 125 km) and to 1 km for long range (i.e., 250 km) scans, the latter being carried out only twice per hour. Time sampling of radar volume data is such that there are 4 acquisitions per hour (i.e., every 15 min). Procedures to correct for gas absorption, to remove ground clutter echoes and to identify anomalous propagation conditions are routinely applied (Alberoni et al., 2001).

In the next three sections an example of weather radar acquisitions will be shown, the algorithm to classify the radar volume into microphysical species described, and the radar simulator for COSMO-LAMI presented.

3.1 Weather radar reflectivity measurements

In order to exploit the polarization capability of both SPC and GAT radars, we have used the measured radar reflectivity factor at horizontal (h) and vertical polarization (v), i.e. $Z_{hh}(r,\theta,\varphi)$ and $Z_{vv}(r,\theta,\varphi)$, where r is the range (km), θ (deg) the elevation angle and φ the azimuth angle (deg). For the purpose of this paper, only the Z_{hh} and Z_{dr} radar observables, being the latter the ratio between the horizontal and the vertical polarization component of the radar reflectivity factor, have been used. The differential phase measurements, useful to correct for path attenuation, were not available for SPC and GAT radars. However, due to the availability of two weather radars looking at a common region, the data volume of SPC radar has been mosaiced exploiting the GAT data volume and taking the maximum of reflectivity between the two overlapped observations (Marzano et al., 2007). The basic assumption we have made is that the aforementioned strategy corresponds to the most unattenuated observation.

Examples of Range-Height Indicators (RHIs) and Plan Position Indicators (PPIs) of radar measurements, collected at 16:30 and 18:30 UTC on 20 May 2003 from SPC radar in terms of Z_{hh} and Z_{dr}, are shown in Figs. 4 and 5, respectively. RHIs have been obtained at the azimuth angle φ=280° from the North, that is along the line of sight between the two radars (indicated with a black filled circle in Fig. 5), whereas the PPIs

ACPD
10, 20461–20514, 2010

have been obtained at the elevation angle of θ=3° in order to avoid the radar beam blockage due the Apennine Mountains chain in the south west region.

On the right panels of the Figs. 4 and 5, respectively, the RHIs and PPIs of the classified radar volume and the estimated water content are shown as well. The details about the adopted classification procedures of hydrometeors and their estimation of water content will be briefly discussed in the next section. For an exhaustive discussion, see Marzano et al. (2008).

From Figs. 4 and 5 a deep convective event in the flat lands of North-East Italy within the area covered by the two radars, probably due to a cold and dry air intruding from North-East and moving across the Alps, can be identified. Local authority reported an intense hailstorm lasting for some hours in this region. The storm maximum development was registered at 16:30 UTC and it was located approximately at 55–60 km from SPC and 30–35 km from GAT. The storm slowly moved eastward (13.3 km/h), as the two time steps for both RHI and PPI imply (Fig. 4), because of the easterly flow at the low levels slowing down its passage. Moreover, at 16:30 UTC the vertical structure of the cell clearly shows hail in the inner core, up to 5–6 km, associated with a highly localized cell with a plume reaching 11.5 km which suggests a strong updraft; a more widespread structure is detected by the radar, at 18:00 UTC, associated with a reduction of the hail content and the maximum height of the plume reaching 10 km.

3.2 Radar-based retrieval of microphysical features

In order to evaluate the models microphysics, some information about the microphysical composition of the portion of atmosphere covered by the radars of SPC and GAT are needed. In the following, the Bayesian Radar Algorithm for Hydrometeor Classification at C-band (BRAHCC) algorithm and the water content estimator, described in Marzano et al. (2008), are briefly summarized. The basic idea of BRAHCC is that a radar resolution volume can be characterized both by radar observables and external meteorological information, like temperature. The use of Bayesian theory and of radar signatures together with auxiliary information, provide the ingredients to perform the

ACPD
10, 20461–20514, 2010

hydrometeor classification by BRAHCC.

A radar resolution volume (range bin) can be characterized by a column vector $\boldsymbol{x}$, which includes both radar and possible meteorological observables, such as co-polar reflectivity Z_{hh}, differential Z_{dr}, and specific differential phase Kdp and local temperature T. Within the Bayesian theory, assigning correct hydrometeor classes to radar bins implies the knowledge of a posteriori (or posterior) conditional probability density functions $p(c_i|\boldsymbol{x})$, where c_i is the unknown hydrometeor class with $i=0,\ldots,N_c$ and N_c the number of classes. The Maximum A Posteriori (MAP) decision rule is quite intuitive, as the hydrometeor class is provided by the index c_i that maximizes the conditional posterior PDFs:

$$\boldsymbol{x} \in c_i \Leftrightarrow p(c_i|\boldsymbol{x}) > p(c_j|\boldsymbol{x}), \quad \forall j \neq i \tag{1}$$

The problem is that conditional posterior probabilities $p(c_i|\boldsymbol{x})$ are usually unknown, but from the Bayes theorem we can express it as a function of the conditional *likelihood* PDF ($p(\boldsymbol{x}|c_i)$) and the a priori (prior) PDF of hydrometeor class c_i ($p(c_i)$) as follows:

$$\boldsymbol{x} \in c_i \Leftrightarrow p(c_i|\boldsymbol{x}) \cdot p(c_i) > p(c_j|\boldsymbol{x}) \cdot p(c_j) \quad \forall j \neq i \tag{2}$$

To solve Eq. (2) both the likelihood and prior PDF must be expressed: this represents one of the most critical issues of a Bayesian approach (Bernardo and Smith, 1994). The simplest choice, usually used to simplify the mathematical treatment of the Bayesian problem (Richards et al., 2006; Lillesand et al., 1994), is to assume a multi-dimensional Gaussian to describe the likelihood PDF. This implies that the polarimetric signatures of hydrometeor classes are hyper-ellipsoids in the multi-dimensional space of the observation space (i.e., the space of the polarimetric signatures). The mean vectors $\boldsymbol{m}_i$ and covariance matrices $\boldsymbol{C}_i$ of the radar observables completely describe the multidimensional Gaussian PDF for each class, and they can be estimated by exploiting radar backscattering simulations. On the other hand, the a priori PDF $p(c_i)$ may be used to incorporate any a priori knowledge about the hydrometeor classes. In lack of further information, we have simply exploited temperature to suppress some

ACPD
10, 20461–20514, 2010

hydrometeor classes that we believe cannot exist outside a given temperature range, following what was suggested by Marzano et al. (2007) and Zrnić et al. (2001).

Under the previous hypothesis, done on $p(\boldsymbol{x}|c_i)$ and $p(c_i)$, Eq. (2) becomes equivalent to minimizing a quadratic *distance* function $d(\boldsymbol{x},c_i)$ with respect to c_i and dependent from $\boldsymbol{m}_i$ and $\boldsymbol{C}_i$ which can be directly computed from the radar observables. As already stated, the knowledge of the class c_i for each bin of the radar volume is not simple to assimilate into weather forecast models. To overcome this difficulty an estimate of the water content of hydrometers (W) has been accomplished, as in Marzano et al. (2008), exploiting the following power relation:

$$W \cong a' Z_{\mathrm{hh}}^{b'} Z_{\mathrm{dr}}^{c'} \tag{3}$$

where a', b' and c' are the proper regression coefficients obtained simulating W, Z_{hh} and Z_{dr} by means of the backscattering model at C band.

The results obtained applying the BRAHCC algorithm and the water content estimate on the case study on 20 May 2003 are shown in the right panels of Figs. 4 and 5 as RHIs and PPIs. In this plots the classes c_i, with i ranging from 0 to 12, are specified as follows: LD (*large drops*, i=0), LR (*light rain*, i=1), MR (*medium rain*, i=2), HR (*heavy rain*, i=3), H (*hail*, i=4), G/SH (*graupel/small hail*, i=5), DS (*dry snow*, i=6), WS (*wet snow*, i=7), IC (*ice crystals*, i=8). The vertical sections of the classified radar volume, shown in Fig. 4, seems to confirm the presence of hail at ground, as reported by local direct observations, between about 16:30 and 18:00 UTC. Indeed at 18.00 UTC the event seems to become weaker both in terms of radar reflectivity and hail at ground. Therefore, because of the un-attenuated LAM model results, attenuation-corrected radar data are used in what follows in order to facilitate the comparison between the models and the radar observation.

3.3 Radar response numerical simulator

Simulated weather radar data have been generated by means of the radar simulator model polarized-version (RSM-POL) (Marzano et al., 2007; Molini et al., 2009).

ACPD
10, 20461–20514, 2010

Starting from the radar model, developed by Haase et al. (2000), RSM-POL has been enhanced with a polarimetric module in order to compute some dual polarized variables, such as copolar vertical reflectivity and differential reflectivity and (Z_{vv},Z_{dr}). The atmospheric variables, needed to simulate the electromagnetic signature of the different hydrometeor types, are part of the three-dimensional (3-D) output fields, simulated by COSMO-LAMI and, in particular: rain sedimentation flux, snow sedimentation flux, graupel sedimentation flux, temperature, pressure, cloud ice specific content, cloud water specific content, the water vapor ratio and number density intercept parameter N_0^i for each species i.

RSM-POL is able to take into account a wide range of features related to the propagation of an electromagnetic wave through the atmosphere. Gaseous absorption effect is reproduced by using the millimeter-wave propagation model of Liebe et al. (1989) which allows to consider the effects of absorption by atmospheric gases (e.g., molecular oxygen, water vapor and nitrogen); scattering reflectivity factors for non spherical particles have been calculated following the T-matrix approach (Mackowski and Mishchenko, 1996). The RSM-POL provides simulated PPI or RHI scans, considering the radar beam geometry and its effects on measurements; furthermore, RMS-POL's modularity allows evaluating separately the contribution of each microphysical species in terms of their own peculiar reflectivity as it would be if single species electromagnetic responses were reciprocally independent.

4 Mesoscale non-hydrostatic models

To better investigate the role of microphysics within numerical weather prediction models, two mesoscale models are used. The COSMO-LAMI has been originally developed by Deutsche Wetterdienst (DWD), the German National Weather Service, and is currently run by the Italian Air Force in Italy; the MM5-V3 has been developed by Penn State University and National Center for Atmospheric Research (PSU/NCAR) and daily run in Italy by CETEMPS at the University of L'Aquila. A brief description of both COSMO-LAMI and MM5-V3 is given below.

ACPD
10, 20461–20514, 2010

4.1 COSMO-LAMI mesoscale forecast model

The COSMO-LAMI (Doms and Schättler, 1999) is a non-hydrostatic and fully compressible numerical weather prediction model. The primitive hydro-thermodynamic equations are used to describe compressible non-hydrostatic flow in a moist atmosphere without any scale approximation. The model uses hybrid terrain-following coordinates, while the vertical resolution may be varied from a value of 50 m near surface up to several hundred meters according to altitude. For this study, COSMO-LAMI has been run with three different one-way nested domains having resolution of 7, 2.8 and 1 km and 50 vertical levels. The COSMO-LAMI model has the feasibility of several turbulent, surface and microphysical schemes. For a more comprehensive description of the model, the reader can refer to Steppeler et al. (2003). In this study the following model set up is used: the 2.5 order local closure scheme of Mellor-Yamada for the PBL; the Kain-Fritsch (Fritsch and Kain, 1993) parameterization for the convection for the domain at 7 km only; a bulk microphysics parameterization including water vapor, cloud water, rain, and snow. A cloud-ice scheme including graupel (Reinhardt and Seifert, 2006) is also used. The basic prognostic model variables are wind vector, temperature, pressure perturbation, specific humidity, rain water, cloud liquid water, cloud ice, snow and graupel content.

4.2 MM5-V3 mesoscale forecast model

The MM5-V3 is a non-hydrostatic model at the primitive equations (Dudhia, 1993 and, Grell et al., 1994) in terrain following vertical coordinate (sigma). Four two-way nested domains are used in this study, with the innermost (1 km resolution) covering the whole GAT-SPC range. It has to be noticed that MM5-V3 high resolution domain is smaller than the COSMO-LAMI one, but this will not influence the results of the comparison. Thirty-three vertical sigma levels unequally spaced, with the higher resolution in the lower layers, are used for MM5-V3. The MRF (Troen and Mahrt, 1986; Hong and Pan, 1996) parameterization for the PBL is used. This is a first order non-local closure

ACPD
10, 20461–20514, 2010

scheme. The Kain-Fritsch (Fritsch and Kain, 1993) cumulus convection parameterization is used only for domain 1 and 2; no cumulus scheme is used for domains 3 and 4. An explicit computation of hydrometeors is also used; the microphysics scheme is the Reisner "graupel included" scheme (Reisner et al., 1998) having a snow intercept parameter depending on temperature (Thompson et al., 2004).

The most important differences between the two non-hydrostatic models are summarized in Table 1.

4.3 Microphysics related to the experiments

Generally, NWP mesoscale models accounts for four hydrometeors: cloud water q_c, rain q_r, cloud ice q_i, and snow q_s.

Heavily rimed ice particles like graupel and hail are commonly found in deep convection; the thermo-dynamical processes associated with their conversion have to be correctly accounted for reproducing the convection. An inverse-exponential size distribution is used in COSMO-LAMI (Reinhardt and Seifert, 2006 hereafter RS06) for all hydrometeors, the one for graupel being:

$$f_g(D_g) = N_0^g \exp(-\lambda_g D_g) \tag{4}$$

where $N_0^g = 4 \times 10^6\ \mathrm{m}^{-4}$ (Rutledge and Hobbs, 1984) is the standard value for the intercept parameter, and D_g is the diameter of the graupel particle. The mass-size distribution follows a standard power-law in COSMO-LAMI, as well as for the terminal fall velocity:

$$m_g = c_g^m D_g^e \tag{5}$$

$$v_T^g(D_g) = a_g^0 D_g^b \tag{6}$$

with the default values of the parameters corresponding to the experiment 3 (Table 2, $c_g^m = 169.6$, $a_g^0 = 442.0$, $b = 0.89$ and $e = 3.1$ in SI units.)

ACPD
10, 20461–20514, 2010

A generalized gamma distribution for each hydrometeor, except snow (Thompson et al., 2006), is used for MM5-V3:

$$N(D) = \frac{N_t}{\Gamma(\mu+1)} \lambda^{\mu+1} D^{\mu} e^{-\lambda D} \quad (7)$$

where N_t is the total number of particles in the distribution, D is the particle diameter, λ is the distribution slope and μ is the shape parameter. The mixing ratios of cloud water, rain, cloud ice, snow and graupel are explicitly computed, whereas the number concentration of cloud ice only is predicted. This implies a double-moment scheme for cloud ice only. Snow distribution is given by the sum of an exponential and a gamma distribution (Thompson et al., 2006).

A standard power law, similar to the one for COSMO-LAMI (Eqs. 10a and b), is used to reproduce the mass and terminal velocity of each hydrometeor. To analyze the role of the graupel parameters in both models, several different values of intercept N_0^g, density ρ_g and velocity deposition parameters have been selected for the two models following Gilmore et al. (2004), as will be discussed in the next section.

The European Centre for Medium-Range Weather Forecast (ECMWF) analyses at 0.25° are used to initialize and upgrade the boundary conditions, for both models. All the simulations start at 00:00 UTC of 20 May 2003 and last for 24 h.

5 Sensitivity analysis

The hailstorm event described in Sect. 2 is here used to investigate the role of hail/graupel species for both amount and type of precipitation reaching the ground, and the intensity of deep convective processes.

5.1 Design of NWP model experiments

Following Reinhardt and Seifert (2006) and Gilmore et al. (2004), several simulations (called, "experiments" 1 to 9) are performed using different graupel/hail microphysical settings:

ACPD
10, 20461–20514, 2010

1. values ranging from 4×10^4 to 4×10^6 m^{-4} for the intercept parameter N_0^g;

2. values ranging between 0.2 to 0.9×10^6 g/m^3 for the density ρ_g of the graupel particle size;

3. several values of the velocity-size/mass-size relationships.

Small N_0^g and large values of density change the properties of the particle ensemble: more hail-like behavior appears, particles do fall faster and melting is reduced, so that melted graupel/hail cannot reach the ground (Lin et al., 1983; Chen et al., 1985; Heymsfield and Kajikawa, 1987). The different microphysical settings are described in table 2 where a_g^0, b, e, c are the parameters of Eqs. (5) and (6). The final experiment (experiment 10) is performed to test the sensitivity of both models to the deposition velocity, based on the Gilmore et al. (2004) results. In their experiments graupel reached the ground, using both a smaller N_0^g and a larger depositional velocity than the ones used for the experiments 1–9 analyzed in this study. Therefore, experiment 10 is performed with the aim of exploring the upper limit of the depositional velocity. As it will be shown, this setting allows graupel to reach the ground; the same setting is used for both models, in order to facilitate the comparison. Moreover the detected snow aloft supported the choice of exploring values ($\rho_g=0.2\times10^6$ g/m^3 and $N_0^g=10^4$–10^5 m^{-4}) which included snow.

The three-dimensional microphysical structure of the simulated (COSMO-LAMI and MM5-V3) deep convective atmosphere has been compared to those provided by the meteorological radar retrievals. For each experiment the comparison is performed in terms of horizontal (at ground-level) and vertical radar reflectivity, vertical profiles of the different microphysical species and microphysical columnar contents. Furthermore, a spectral analysis is performed to objectively investigate the simulated 3-D convective flow field sensitivity to the microphysical settings using the radar data.

ACPD
10, 20461–20514, 2010

5.2 Analysis of the convective cell horizontal position

A preliminary analysis of the cell position for each experiment is here performed by varying the microphysical parameters. The position of the most intense convective cell is assessed for both LAM models by identifying the coordinates where the maximum vertical velocity occurs, considering only the overlapping area of the two radar coverage. The cell that was actually observed by the radars is located approximately half way along the imaginary line connecting the two radar positions (GAT and SPC, Fig. 6 red line). Different model parameterizations lead to different cell positions; somehow, the different cell position permits to highlight the role of the microphysical parameters in timing and location of the cell for both models. A slightly more widespread cells position for COSMO-LAMI than MM5-V3 (Fig. 6 lower and upper panel, respectively) is found.

Experiments 2–4, and 6 for COSMO-LAMI produce the cell between the two radars at approximately 17:00 UTC, but south of the alignment between the radars; whereas, the other experiments (1, 5, 8, and 9) clearly result in a cell with a wrong position. Only experiment 7 produces the cell along the alignment of the two weather radars, approximately in the right position. All these experiments delay the convective cell development by approximately 30 min.

Most of the MM5-V3 experiments (1, 2, 4–7 and 9) yields the convective cell near the observed one, but also in this case southward with respect to the alignment between the two radars. Experiment 8 produces the cell in a wrong position, as well as for experiment 3 where the cell is misplaced too westward. Only experiment 10 yields the cell close to the observed one. The timing of the cells for all the experiments is delayed of 1 h, except for experiment 6 in which the cell breaks out at the right time (16:30 UTC), yet in the wrong position. The differences in the cell position in space and time for both models is probably due to the different microphysical parameters which influences also the dynamics of the two NWP models.

ACPD
10, 20461–20514, 2010

5.3 Radar reflectivity horizontal and vertical field analysis

The radar reflectivity at the ground and the vertical distribution produced by the two NWP models is compared with the two weather radar observations in order to explore a probable different response between the two. The reflectivity maps will be analyzed for all simulations, but for both models only the results of the best run will be shown: experiment 7 and 10, respectively for COSMO-LAMI and MM5-V3. Reflectivity maps are obtained using the RMS-POL simulator described in Sect. 3.3 for COSMO-LAMI, whereas for MM5-V3 an off line and without the radial geometry procedure is applied (De Sanctis, 2008).

Reflectivity shows poor sensitivity to the microphysical parameters for COSMO-LAMI. The ground reflectivity is similar for most of the settings (1–6, 8 and 9) except for experiment 7 which shows a structure in good agreement with the one detected by the radars. Besides the similarity for the horizontal structure of the cell among the various experiments, the vertical structure is clearly different. Setting 1 produces a multicellular structure which is not observed; moreover, the cells are misplaced if compared to the observed one. The vertical structure of experiment 2 shows a very well developed cell reaching the ground at 17:15 UTC in its final stage, having a 45-min delay with respect to the observation. Yet, its vertical structure agrees well with the observation reaching a height slightly higher than the observed one. Unfortunately, this experiment does not produce a horizontal reflectivity map comparable with the observed one. Both experiments 3 and 4 produce a cell reaching the ground, but the cell is too large for the first one and in the wrong position for the second one. Experiment 5 produces a cell reaching the ground but poorly defined, whereas experiment 6 produces an eastward misplacement of the cell, at least at upper levels. Both settings 8 and 9 produce two cells. Reflectivity maps for COSMO-LAMI for experiment 7 (best run) clearly show the precipitating system crossing the Po Valley and moving eastward (Fig. 7 left upper panel) and the cell reaching the maximum intensity (orange spot along the alignment between the radars in Fig. 7 left lower panel), only half hour later than the observed one (Fig. 5

ACPD
10, 20461–20514, 2010

upper panels) but underestimating the maximum reflectivity of approximately 10 dBZ. The COSMO-LAMI response to the different settings agrees with what previously found by Reinhardt and Seifert (2006) for an idealized 3-dimensional convective experiment. In fact, Reinhardt and Seifert (2006) found precipitation at the ground maximized only for small graupel intercept parameter and large density: $N_0^g=10^4$ (m^{-4}) and $\rho_g=0.9$ (10^6 g/m^3). Also in this study the small intercept parameter and large density (experiment 7) produces the best ground response in terms of reflectivity, for what concerns COSMO-LAMI.

As far as MM5-V3 is concerned, setting 1 produces a cell which is not aligned with the two radars; the reflectivity map does not agree with the observed one and reflectivity is underestimated. Moreover, the cell produces a maximum of reflectivity between 2 and 4 km, with a maximum vertical development of 10 km. Settings 2–8 do not produce any reflectivity at the ground, and the cell is misplaced similarly to setting 1. The base of the cell for these settings (2–8) varies from 0.5 km to 5 km (respectively 7 and 8), but the vertical distribution of reflectivity is well in agreement with the observed one, except for setting 8 which underestimates the reflectivity Finally, experiment 9 produces a reflectivity map which agrees with the radar for both distribution and intensity, with a vertical structure in agreement with the observed one. But the cell is misplaced if compared to the alignment of the two radars. The MM5-V3 reflectivity maps for experiment 10 (best run), which is based on setting 9 but using a faster deposition velocity, clearly show the system starting to develop at 16:30 UTC northbound of the two radars (Fig. 7 right upper panel). In the following hour (at 17:30 UTC), that is one hour later than the observed one (Fig. 5 upper panels), it reaches the maximum stage (Fig. 7, right lower panel) in the right position, but an underestimation of approximately 10 dBZ is produced. The experiment 10 is characterized by large density and large intercept parameter: $N_0^g=10^6$ (m^{-4}) and $\rho_g=0.9$ (10^6 g/m^3) which allowed producing precipitation at the ground, hence a good response compared to the ground reflectivity.

In summary, MM5-V3 produces a different result from COSMO-LAMI. Indeed, for both NWP models a large particle density is required to produce the best ground

ACPD
10, 20461–20514, 2010

response, even if the intercept parameter for MM5-V3 is larger than for COSMO-LAMI. The different responses to the vertical structure of the convective cell for the two best runs deserve a further analysis. A cross-section along the two radars alignment is taken at the same time steps as for Fig. 7 for both NWP models.

The cross section for COSMO-LAMI shows the early stage of the cell at 16:45 UTC (Fig. 8 upper left panel), reaching the mature stage at 17:00 UTC at approximately 40 km away from SPC (Fig. 8 middle left panel). Therefore, a good agreement between COSMO-LAMI and radar observations (Fig. 4 left panel) is obtained, but the cell remains smaller than the observed one. The cell's maximum intensity as well as its maximum height are correctly reproduced (Fig. 8 lower left panel), but high values of reflectivity reach higher height than observed (Fig. 4 left panel). The cell reaches its final development stage at 17:15 UTC (Fig. 8 lower left panel).

For what concerns MM5-V3, the time sequences of the cell for setting 10 show echoes only at 5km altitude (Fig. 8 upper right panel, 16:30 UTC), suggesting a clear delay in the cell development with respect to the radar observation (Fig. 4 left panel). Indeed, the cell develops at approximately 17:00 UTC reaching a height of 8 km (Fig. 8 middle right panel) and the mature stage one hour later (at 17:30 UTC, Fig. 8 lower right panel). Anyway, the cell is located slightly westward than the observed one. The maximum radar reflectivity is in good agreement with the observed one, whereas the maximum height is slightly smaller than the observed one (Fig. 4 left panel).

Both NWP models attempt to produce a double cells structure as eventually the weather radar detected; nevertheless, the second cell is much weaker than the first one.

5.4 Hydrometeor columnar content analysis

5.4.1 Mean vertical structures of hydrometeors content

In order to further evaluate the impact of the different settings, the mean columnar content of the convective cell for each hydrometeor and each setting has been analyzed.

ACPD
10, 20461–20514, 2010

As expected, the average vertical profiles of water content for three classes of hydrometeors, namely graupel, rain and snow, (which have been retrieved from radar observation) reveals that the graupel distribution (Fig. 9 red line) characterizes this event. A relative maximum at about 7.5 km and a minimum positioned at 2.5 km is observed for graupel: a deep layer of graupel content of 0.4 g/m^3 is reached at approximately 7.5 km; between 2.5 and 6.5 km a graupel content of 0.2 g/m^3 is detected, and a maximum content larger than 0.8 g/m^3 is observed down to the surface. Snow is detected only above 1.5 km with a content of 0.1 g/m^3 up to 3.5 km, and decreasing at upper levels (Fig. 9 green line). Although smaller than graupel, rain content too is recorded at the surface (Fig. 9 blue line) and rapidly decreasing at upper levels. No rain is detected above 4 km.

The graupel profile shows a considerable amount reaching the ground, which confirms the experimental evidence of a graupel event. It should be noticed that residual radar attenuation effects could explain the relatively low value of about 0.18 g/m^3 for graupel at height of approximately 2.5 km. Therefore, the small attenuation may be a concurring factor to explain the differences between simulations and observations. On the other hand, evidence of graupel reaching the ground is directly reported after the storm. The vertical distributions of the hydrometeor content for both NWP models show large sensitivity to the different settings. Low density values associated with N_0^g ($=4\times10^4$ m^{-4}) produce a large underestimation of all hydrometeors for COSMO-LAMI (run 1, Fig. 10a). The increase of the intercept (run 2) results in a large increase of all hydrometeors, allowing the model to reach a good agreement with the observation (Fig. 10a); but the graupel maximum is present at lower level (Fig. 10a, run 2) than the observed one. A further increase of N_0^g produces an overestimation of snow and an underestimation of rain for COSMO-LAMI (Fig. 10a, run 3). A doubling of ρ_g (0.4×10^6 g/m^3, run 4, Fig. 10a) largely increases snow (with respect to run 1) producing overestimation as for run 3. The increase of N_0^g produces a dramatic reduction of all hydrometeors (run 5, Fig. 10a), turning into a large underestimation. This is only slightly recovered by a further increase of N_0^g, as for run 6 (Fig. 10a). Run 7, the best run based

ACPD
10, 20461–20514, 2010

on the comparison with the radar reflectivity at ground, produces an overestimation of snow and an underestimation of graupel (Fig. 10a, red line). If N_0^g is kept constant (we move along the lower row of Fig. 10a, from the left to the right) the increase of ρ_g produces a gain of snow and graupel (run 4), whereas a further increase of ρ_g produces a reduction of both graupel and rain, and a gain of snow (run 7). The increase of N_0^g (run 8, Fig. 10a) partly allows recovering the large snow overestimation, but both graupel and rain are reduced compared to run 7. The further increase of N_0^g considerably reduces all hydrometeors producing underestimation for all of them (Fig. 10a, run 9). Finally, experiment 10 clearly shows an expected impact: a large reduction of the graupel concentration (by melting), and indeed a large increase of the rain content (Fig. 10a, COSMO-LAMI). Snow is also largely reduced. Therefore, for what concerns COSMO-LAMI, setting 2 is the only one producing an event characterized by graupel, even if they barely reach the ground (see discussion in next par. Fig. 12). Moreover, the reflectivity at the ground for setting 2 is not as good as for setting 7. On the other hand, the vertical profile clearly supports the hypothesis of a snow event for setting 7, but a large underestimation of graupel reaching the ground is found. Based on these results, it can be inferred that the good agreement between setting 7 and observations, in terms of ground reflectivity, is mostly produced by snow. Reinhardt and Seifert (2006) found setting 7 as the best one for producing surface precipitation in an idealized 3-dimensional convective case. The event of isolated convection analyzed in this study did not produce the same results of Reinhardt and Seifert (2006), a conclusion which is not surprising because of the higher complexity of real convective events.

For what concerns MM5-V3, the low density values (ρ_g=0.2×10^6 g/m^3, settings 1–3, Fig. 10b) produce a large underestimation of the graupel content compared to the observed one (Fig. 10b red line) only for N_0^g=4×10^4 m^{-4} (run 1, Fig. 10b, red line). The snow content decreases when increasing N_0^g from 10^4 to 10^5 m^{-4} (run 2), whereas a gain is obtained for a further increase of N_0^g (run 3, Fig. 10b). The rain content is largely underestimated and it does not reach the ground except for setting 1, i.e. for a small intercept value. Among these three settings none of them reproduces a vertical

ACPD
10, 20461–20514, 2010

distribution in good agreement with the observed one (Fig. 10b, red line). In order to evaluate the impact of the density increase (up to ρ_g=0.4×10^6 g/cm^3) run 4 is compared with run 1 (Fig. 10b, red line). A large reduction of all hydrometeors content is produced: approximately, 1/2 of the graupel, 1/20 of snow and 1/5 of rain is obtained by increasing ρ_g. The increase of the intercept (setting 5 against setting 4) only allows for a gain of rain (Fig. 10b). A further increase of N_0^g produces a large decrease of all hydrometeors and a vertical distribution which is completely different from both the others and the observed one. The biggest density value (ρ_g=0.9×10^6 g/cm^3, run 7–9, Fig. 10b) shows an increase of the all hydrometeors if N_0^g increases; it ends up with both graupel and snow content overestimated, and rain underestimated. The increase of deposition velocity (run 10 for MM5-V3, Fig. 10c) permits to reduce both the graupel content and the maximum height. This turns in a maximum value of graupel in good agreement with the observed one at upper levels, but largely underestimated at lower ones. Also the snow content is reduced, but still overestimated (maximum value of 0.35 g/m^3 against 0.1 g/m^3 observed); moreover its vertical distribution is different from the observed one. The rain content is in good agreement with the observed one (0.27 g/m^3 of the run 10 against 0.4 g/m^3 observed).

In summary, the analysis, carried out by this study, highlights that the vertical structure of the hydrometeors largely changes depending on the graupel density and the PSD intercept value, as it was expected. Beside of the fair agreement of the vertical structure all hydrometeors with the observed one for settings 3 and 2 for MM5-V3 and COSMO-LAMI, respectively, the results of the comparison with the ground-measured values are not the same for these experiments. Indeed, based on the comparison between radars and NWP models near-surface reflectivity, a good agreement is found for settings 7 and 10 for COSMO-LAMI and MM5-V3, respectively. This suggests that the NWP model precipitating species (specifically rain), which eventually are in good agreement with the observed pattern, are incidentally obtained for the wrong reason. Therefore, it is extremely important to verify the vertical structure of the NOW models products in order to correctly reproduce the hydrometeor spatial distribution.

ACPD
10, 20461–20514, 2010

5.4.2 Hydrometeor category analysis

The analysis of the columnar content of three hydrometeor categories (hail, snow and rain) has been performed using the cross section along the two weather radars alignment (along the red line in Fig. 6) and the horizontal distribution at the ground. The best runs in terms of ground effects and vertical structure, i.e. simulations 7 and 2 and 10 and 3, respectively, for COSMO-LAMI and MM5-V3, will be used. In order to facilitate the comparison between radar observations and NWP models, the radar-derived hydrometeors are degraded to three main categories: *snow* (green in the next figures) which accounts for dry snow and ice; *graupel* (red in the next figures) which accounts for hail, graupel and small hail; *rain* (blue in the next figures) which accounts for light drizzle, and light, moderate and heavy rain. The comparison with the model products is now straightforward. The radar products clearly show a band of *graupel* reaching the base scan, hence we can reasonable assume that *graupel* reach the ground together with *rain* (Fig. 11 upper left side).

The best run (setting 7) for COSMO-LAMI clearly shows (Fig. 12 left side, middle panel, green) *snow* at higher levels in good agreement with observations, whereas *graupel* are produced only at approximately 5000 m and they are underestimated (Fig. 12 left side, middle panel, red). Moreover, only *rain* is found at ground (Fig. 12 left side, middle and bottom panels, blue), whereas *graupel* is detected by the weather radars and reported from local authority too. The vertical distribution of the water content (Fig. 12 left side, upper panel) is generally overestimated at upper levels, whereas it is correctly reproduced at the lower ones. The vertical structure of setting 2 shows both a *graupel* core (Fig. 12 right side, middle panel, red) larger than the setting-7 one and a smaller amount of *rain* reaching the ground (Fig. 12 right side, middle panel, blue). Generally speaking, a good agreement with the observed vertical structure is found, whereas a large underestimation of the ground observations (Fig. 12 right side, bottom) is note.

ACPD
10, 20461–20514, 2010

The vertical distribution of hydrometeors for MM5-V3 (setting 10) well agrees with the radar one. *Snow* is produced between 3000 and 10 000 m (Fig. 13 left side, middle panel, green), whereas it is observed between 6500 m and 10 000 m. A good agreement is found for *graupel* too: they are produced between 2000 and 8000 m by MM5-V3 setting 10 (Fig. 13 left side middle panel, red), whereas they are observed between 1000 and 8000 m (Fig. 11 left side upper panel, red). Therefore, MM5-V3 tends to correctly produce *graupel*, even though it is not present at ground (Fig. 13 left side middle panel, red color) where it is actually observed. Finally, the MM5-V3 near-surface distribution for *rain* fairly well agrees with the radar observed one (Fig. 13 left side lower panel, blue). The previous good agreement between MM5-V3 and radar observations is confirmed by the hydrometeor water content along the cross-section between the two radars, even though an overestimation is produced by MM5-V3 (3.5 g/m^3, Fig. 13 left side upper panel) with respect to radar (0.5 g/m^3, Fig. 11 left side lower panel). The horizontal distribution of hydrometeors confirms what found for the vertical distribution. The best run (experiment 10) for MM5-V3 is clearly characterized by *rain* at ground which is not what weather radars detected (Fig. 11 right side upper panel). On the other hand, MM5-V3 horizontal distribution is in very good agreement with what observed by radars (Fig. 11 right side upper and lower panels): similarly to the observation, a "banana shape" structure is produced, even if the overestimation of the water content (Fig. 13 left side lower panel), together with the characterization of the event as a *rain* one, are still present. Unfortunately, for what concerns run 3, a large core of *snow* is produced instead of *graupel* (Fig. 13 right side, middle panel, green and red, respectively) and *graupel* tends not to reach the ground. This is also confirmed by the horizontal distribution of the hydrometeors at the ground: clearly only a small amount of *rain* reaches the ground (Fig. 13 right side lower panel). The cross section for the water content shows an overestimation (Fig. 13 right side upper panel) at upper levels, whereas a good agreement is found at lower levels.

In summary, COSMO-LAMI clearly produces *snow* associated with a large underestimation of *graupel*, both ice hydrometeors are not able to reach the ground. Similarly,

ACPD
10, 20461–20514, 2010

MM5-V3 produces *snow* and *graupel* at upper levels, but the deposition velocity does not allow them to reach the ground without melting, even in the case of a faster deposition velocity (like in the best run – setting 10).

5.5 Spectral analysis of hydrometeor spatial fields

The Fourier spectral analysis of the integrated water content for the different hydrometeor species, produced by all numerical experiments and detected by the polarimetric radars, has been carried out in order to objectively compare the results of the different settings. The Fourier analysis allows to identify NWP models difficulties in partitioning energy at different scales. The analysis is performed by applying the Fast Fourier Transform (FFT) algorithm to the volume scan by both radars at the time of the maximum cell development for each setting.

The spectral analysis clearly shows a different response for both models and radar observations at the two sites (Fig. 14a and b left and right panels). Indeed, it seems that the volume, scanned from the two radar sites, leads to a different spectral behavior (compare the red lines Fig. 14 left and right panels). Moreover, a different response is obtained for the three types of hydrometeors, with *snow* showing the largest discrepancies between observations and both COSMO-LAMI (Fig. 14a middle panels) and MM5-V3 (Fig. 14b middle panels).

For what concerns COSMO-LAMI, *graupel* show a variance larger than the one observed at GAT for all settings, but producing a slope at large scale (down to 9 km) similar to the observation. At scale from 9 km to small scale (Fig.14a upper panel left side) differences between the model slope and the one observed at GAT are clearly noted (the red line crosses the model ones, Fig.14a upper panel left side). This suggests a NWP model tendency to aggregate *graupel* at small scale. From the SPC site, the variance of the different settings is similar to the observed one (the red line lies down among the model ones Fig.14a upper panel right side). But similarly to GAT, the differences among the slopes at small scale are bigger than at the large one (Fig.14a upper panel right side). *Snow* does not show difference between the two points of view

ACPD
10, 20461–20514, 2010

(GAT and SPC) and also among the settings: a large overestimation of the variance is produced by all settings (Fig. 14a middle panel right and left side). The rain spectra show similarities with the *graupel* one (Fig.14a lower panel right and left side), however differences between COSMO-LAMI and observations at small scale are larger. Most of the model different settings intersect the observation (Fig. 14a lower panel right side, all color and red line, respectively) whose spectrum at small scale tends to be parallel to the *x* axis for both GAT and SPC. This would suggest a NWP model tendency to largely aggregate (correlate) rain at small scale, which is not for the observation. On the other hand, a similar slope is found for both observation and all the settings at large scale, suggesting that the NWP model correctly aggregates (correlates) *rain* at this scale.

The spectral analysis for MM5-V3 clearly shows large differences between GAT and SPC for *hail*: a larger variance than observed is produced for all settings for GAT (Fig. 14b, left side upper panel), whereas the variance of all settings is similar to the observed one, for SPC (Fig. 14b, right side upper panel). Moreover, for what concerns the slope for *graupel*, most of the MM5-V3 settings show good agreement with the observation at small scale too, except for run 7 at GAT (Fig. 14b green with dot left side). This suggests a MM5-V3 good ability in disaggregating graupel at small scale, especially for settings 6 and for the best run (Fig. 14b left side upper panel green and cyan, respectively). Similarly to COSMO-LAMI, MM5-V3 shows difficulties in correctly reproducing *snow*: for both GAT and SPC a larger variance than the observed one and a different slope are produced (Fig. 14b middle panel left and right sides). Finally, the *rain* spectra provide a more complex response: the observed variance is overestimated by most of the settings; the slope shows large differences among the settings for both GAT and SPC (Fig. 14b lower panel left and right sides). Similarly to COSMO-LAMI, MM5-V3 tends to aggregate the *rain* at small scale, but largely enhancing this tendency. All the MM5-V3 settings show a larger slope than the observed at small scale, whereas setting 3 shows an excellent agreement with the observation at scale up to 10.5 km for GAT (Fig. 14b lower panel left side, green and red, respectively). Besides producing

ACPD
10, 20461–20514, 2010

a variance larger than the observed one, the best run well agrees with the observed slope at large scale (Fig. 14b lower panel right side, cyan and red, respectively) for SPC. Noteworthy, setting 6 (Fig. 14b lower panel right side, yellow line) is the only one showing a good agreement with the observation in terms of variance at both scales, whereas for the slope this agreement is found at large scale only.

As final remark, for what concerns MM5-V3 the spectral analysis clearly reveals difficulties in term of energy partition for *rain* and *snow*, whereas mostly for *snow* and *graupel* for COSMO-LAMI.

6 Conclusions

An extensive methodology for investigating cloud-scale microphysics performance of NWP models has been presented. A hailstorm case study been analyzed in terms of dual-poalrized weather radar observations and NWP models. The use of a radar numerical simulator, named RMS-POL, has allowed to compare simulated storms radar signatures (from a suite of sensitivity tests) directly to the polarimetric radar observations. The use of a hydrometeor classification (type/amount) retrieval algorithm, named BRAHCC, applied to both observed and simulated radar data has been used as well to directly compare model simulations and radar observations. Using the above mentioned tools, it has become possible to directly evaluate which set of microphysics treatments may give the NWP simulation closest to the observations in terms of hydrometeor spatial distribution.

A case of deep convection occurred in the Po valley has been used as a benchmark scenario. The analysis has been carried out using data measured by two polarimetric C-band radars (GAT and SPC). The hydrometeor retrieval from the polarimetric radar data has allowed to assess the microphysical structure of the convective cell, revealing the graupel signal from lower up to higher levels. A comparison between two specific NWP model (COSMO-LAMI and MM5-V3) output with the retrieved radar-based products has been performed in terms of vertical and horizontal hydrometeor distribution.

ACPD
10, 20461–20514, 2010

Several NWP models simulations have been performed changing the graupel density, the intercept parameter of the graupel size distribution and deposition velocity; the density has ranged from 0.2 to 0.9×10^6 g/m^3 with N_0^g ranging from 4×10^5 to 4×10^6 m^{-4}.

The comparison between the "observed" microphysical structure and the one produced by the two NWP models settings clearly assess the crucial role of microphysics in reproducing the main features of a deep convective hail-producing cell. Only for specific settings, COSMO-LAMI and MM5-V3 (respectively, settings 7 and 10) are able to produce a cell with evidence of graupel at upper levels (but largely underestimated at the ground) and ground reflectivity in good agreement with the observed one. Also settings 2 and 3, respectively for COSMO-LAMI and MM5-V3, well reproduce the vertical structure, but the ground radar reflectivity for both NWP models does not agree with the observed one. Moreover, besides the good agreement for both NOW models with the observed radar reflectivity pattern, the analysis of the near-surface products has revealed that even the best runs for both NWP models do not agree with what observed: the near-ground product is mostly *rain*, whereas a band of *graupel* detected from radar scans strongly suggests that it has reached ground during the event. This would infer that both NWP models are able to reproduce the structure of the convective cell and the radar reflectivity patterns, but they both are not able to correctly lead to the ground solid hydrometeors. In particular, COSMO-LAMI produces the cell at the right time, but southward than what observed by the radars; MM5-V3 correctly produces the cell along an ideal axis aligned between the two radars, but a delay of more than 1 h for developing the cell is found. The mean vertical structure and the hydrometeor category analysis of the cell for both models reveal a large sensitivity of both NWP models to their implemented microphysics. The latter seems to be largely driven by the graupel density and the PSD intercept value. The positive impact (especially for MM5-V3) of a large depositional graupel velocity suggests that further experiments should be done for investigating heavier and larger graupel. The spectral analysis, performed on the whole volume of the cell, suggests difficulties for both NWP models in partitioning energy for snow for all settings, whereas graupel and rain behave differently depending on

ACPD
10, 20461–20514, 2010

the settings. For COSMO-LAMI a clear tendency to aggregate graupel at small scale is found, whereas all the settings correctly aggregate (correlate) rain at large scale. For MM5-V3 the spectral analysis clearly reveals difficulties in term of energy partition for rain and snow, whereas for graupel a good ability in disaggregating graupel at smaller scale, especially for settings 6 and the best run is found.

In conclusion, this study clearly suggests that the investigations of the mesoscale NWP models microphysics should make use as much as possible of the full set of polarimetric radar observations, focusing mainly on the vertical structure of the cell instead of rain observations near the ground.

Acknowledgements. NCAR (Boulder, CO, USA) is acknowledged for providing the MM5-V3 code. ARPA-SIM (Bologna, Italy) is acknowledged for providing the weather radar data for the analyzed case study. The research project *Proscenio*, funded by the Italian Department of Civil Protection (Rome, Italy), is acknowledged for the general support of this work. The Meteorological Office of the Italian Air Force Office is acknowledged for the use of COSMO-LAMI in a non standard configuration.

References

Alberoni, P. P., Andersson, T., Mezzasalma, P., Michelson, D. B., and Nanni, S.: Use of the vertical reflectivity profile for identification of anomalous propagation, Meteorol. Appl., 8, 257–266, 2001.

Bernardo, J. M. and Smith, A. F. M.: Bayesian Theory, John Wiley & Sons Ltd, New York 608 pp., 1994.

Blossey, P. N., Bretherton, C. S., Cetrone, J., and Khairoutdinov, M.: Cloud-resolving model simulations of KWAJEX: Model sensitivities and comparisons with satellite and radar observations, J. Atmos. Sci., 64, 1488–1508, 2007.

De Sanctis, K.: Mesoscale meteorological modeling at high-spatial resolution: Microphysical sensitivity and polarimetric radar analysis, PhD Thesis at University of Basilicata, 2008.

Doms, G. and Schättler, U.: The Nonhydrostatic Limited-Area Model LM of DWD: Part I. Scientific Documentation, DWD, Offenbach, Germany 172 pp., 1999.

ACPD

10, 20461–20514, 2010

Dudhia, J.: A nonhydrostatic version of the Penn State-NCAR mesoscale model: validation tests and simulation of an Atlantic cyclone and cold front, Mon. Weather Rev., 129, 1493–1513, 1993.

Cheng, L., English, M., and Wong, R.: Hailstone size distributions and their relationship to storm thermodynamics, J. Appl. Meteorol., 24, 1059–1067, 1985.

Cohen, C., and McCaul, E. W.: The sensitivity of simulated convective storms to variations in prescribed single-moment microphysics parameters that describe particle distributions, sizes, and numbers, Mon. Weather Rev., 134, 2547–2565, 2006.

Cotton, W. R., Stephens, M. A., Nehrkorn, T., and Tripoli, G. J.: Colorado State University three-dimensional cloud/mesoscale model – 1982, Part 2, An ice phase parameterization, J. Rech. Atmos., 16, 295–320, 1982.

Droegemeier, K. K., Smith, J. D.,Businger, S., Doswell III, C., Doyle, J., Duffy, C., Foufoula-Georgiou, E., Graziano, T., James, L. D., Krajewski, V., LeMone, M.,Lettenmaier, D., Mass, C., Pielke Sr., R., Ray, P., Rutledge, S., Schaake, J., and Zipserp, E.: Hydrological aspects of weather prediction and flood warnings: Report of the ninth prospectus development team of the US Weather Research Program, B. Am. Meteorol. Soc., 81, 2665–2680, 2000.

Ferrier, B. S., Tao, W.-K., and Simpson, J.: A double-moment multiple phase four-class bulk ice scheme, Part II: Simulations of convective storms in different large-scale environments and comparisons with other bulk parameterizations, J. Atmos. Sci., 52, 1001–1033, 1995.

Garvert, M. F., Woods, C. P., Colle, B. A., Mass, C. F., Hobbs, P. V., Stoelinga, M. T., and Wolfe, J. B.: The 13–14 December 2001 IMPROVE-2 event, Part II: Comparison of MM5 model simulations of clouds and precipitation with observations, J. Atmos. Sci., 62, 3520–3534, 2005.

Gilmore, M. S., Straka, J. M., and Rasmussen, E. N.: Precipitation uncertainty due to variations in precipitation particle parameters within a simple microphysics scheme, Mon. Weather Rev., 132, 2610–2627, 2004.

Grell, G., Dudhia, S., Stauffer, D. R.: A description of the fifth generation of Penn State/NCAR mesoscale model (MM5). NCAR/TN-398+STR, Natl. Cent. For Atmos. Res., Boulder, Colorado, 1994.

Haase, G. and Crewell, S.: Simulation of radar reflectivities using a mesoscale weather forecast model, Water Resour. Res., 36, 2221–2230, 2001.

Hong, S.-Y. and Pan, H.-L.: Nonlocal boundary layer vertical diffusion in medium-range forecast model, Mon. Weather Rev., 124, 2322–2339, 1996.

ACPD

10, 20461–20514, 2010

Fritsch, J. and Kain, J.: Convective parameterization for mesoscale models: the Kain-Fritsch scheme, The Representation of Cumulus in Numerical Models, Meteor. Monogr., No. 46, American Meteorological Society, 165–177, 1993.
Heymsfield, A. J. and Kajikawa, M.: An improved approach to calculating terminal velocities of plate-like crystals and graupel, J. Atmos. Sci., 44, 1088–1099, 1987.
Liebe, H. J.: MPM-An atmospheric millimeter-wave propagation model, Int. J. Infrared Milli., 10, 631–650, 1989.
Lillesand, T. M. and Kiefer, R. W.: Remote Sensing and Image Interpretation, 3rd edn., John Wiley & Sons., Inc. New York, 750 pp., 1994.
Lin, Y.-L., Farley, R. D., and Orville, H. D.: Bulk parameterization of the snow field in a cloud model, J. Clim. Appl. Meteorol., 22, 1065–1092, 1983.
Lynn, B. H., Khain, A. P., Dudhia, J., Rosenfeld, D., Pokrovsky, A., and Seifert, A.: Spectral (bin) microphysics coupled with a mesoscale model (MM5), Part I: Model description and first results, Mon. Weather Rev., 133, 44–58, 2005a.
Lynn, B. H., Khain, A. P., Dudhia, J., Rosenfeld, D., Pokrovsky, A., and Seifert, A.: Spectral (bin) microphysics coupled with a mesoscale model (MM5), Part II: Simulation of a Cape rain event with a squall line, Mon. Weather Rev., 133, 59–71, 2005b.
Luo, Y., Krueger, S. K., and Mace, G. G.: Cirrus cloud properties from a cloud-resolving model simulation compared to cloud radar observations, J. Atmos. Sci, 60, 510–525, 2003.
Luo, Y. L., Xu, K. M., Wielicki, B. A., Wong, T., and Eitzen, Z. A.: Statistical analyses of satellite cloud object data from CERES, Part III: Comparison with cloud-resolving model simulations of tropical convective clouds, J. Atmos. Sci., 64, 762–785, 2007.
May R. M., Biggerstaff, M. I., and Xue, M.: A doppler radar emulator with an application to the detectability of tornadic signatures, J. Atmos. Ocean. Tech., 24, 1973–1996, 2007.
Marzano, F. S., Mugnai, A., Panegrossi, G., Pierdicca, N., Smith, E. A., and Turk, J.: Bayesian estimation of precipitating cloud parameters from combined measurements of spaceborne microwave radiometer and radar, IEEE Trans. Geosci. Remote Sens., 37, 596–613, 1999.
Marzano, F. S., Scaranari, D., Montopoli, M., and Vulpiani, G.: Supervised classification and estimation of hydrometeors from c-band dual-polarized radars: a Bayesian approach, IEEE Trans. Geosci. Remote Sens., 46, 85–98, 2008.
Marzano, F. S., Scaranari, D., and Vulpiani, G.: Supervised classification of hydrometeors using a C-band dual-polarized radar network, IEEE Trans. Geosci. Remote Sens., 45, 3784–3799, 2007.

ACPD
10, 20461–20514, 2010

McCumber, M., Tao, W.-K., Simpson, J., Penc, R., and Soong, S. T.: Comparison of ice-phase microphysical parameterization schemes using numerical simulations of tropical convection, J. Appl. Meteorol., 30, 985–1004, 1991.
Michalakes, J., Chen, S., Dudhia, J., Hart, L., Klemp, J., Middlecoff, J., and Skamarock, W.: Development of a next-generation regional weather research and forecast model, Developments in Teracomputing, edited by: Zweiflhofer, W. and Kreitz, N., World Scientific, 269–276, 2001.
Mishchenko, M.: Diffuse and coherent backscattering by discrete random media-i. radar reflectivity, polarization ratios, and enhancement factors, for a half-space of polydisperse, nonabsorbing and absorbing spherical particles, J. Quant. Spectrosc. Ra., 56(5), 673–702, 1996.
Molini, L., Parodi, A., and Siccardi, F.: An observing system simulation experiment for the study on attenuation of C-band radar measurements, Meteorol. Appl., 15(4), 523–533, 2008.
Morrison, H., Curry, J. A., and Khvorostyanov, V. I.: A double-moment microphysics parameterization for application in cloud and climate models, Part I: Description, J. Atmos. Sci., 62, 1665–1677, 2005.
Proctor, F. H.: Numerical simulations of an isolated microburst, Part I: Dynamics and structure, J. Atmos. Sci., 45, 3137–3160, 1988.
Proctor, F. H.: Numerical simulations of an isolated microburst, Part II: Sensitivity experiments, J. Atmos. Sci., 46, 2143–2165, 1989.
Reinhardt, T. and Seifert, A.: A three categories-ice scheme for LMK, Cosmo Newsletter 6, 115–120, 2006.
Reisner, J., Rasmussen, R., and Bruintjes, R.: Explicit forecasting of supercooled liquid water in winter storms using the MM5 mesoscale model, Q. J. Roy. Meteor. Soc., 124, 1071–1107, 1998.
Richards, J. A. and Jia, X.: Remote sensing digital image analysis: an introduction, 4th edn., Springer-Verlag, Berlin, 476 pp., 2006.
Rutledge, S. and Hobbs, P. V.: The mesoscale and microscale structure and organization of clouds and precipitation in midlatitude cyclones, J. Atmos. Sci., 41, 2949–2973, 1984.
Serafin, S. and Ferretti, R.: Sensitivity of a mesoscale model to microphysical parameterizations in the MAP SOP Events IOP2b and IOP8, J. Appl. Meteorol. Climatol., 46, 1438–1454, 2007.
Smith, P. L., Meyers, C. G., and Orville, H. D.: Radar reflectivity factor calculations in numerical cloud models using bulk parameterization of precipitation, J. Appl. Meteorol., 14, 1156–1165,

ACPD
10, 20461–20514, 2010

1975.
Steppeler, J., Doms, G., Schättler, U., Bitzer, H. W., Gassmann, A., Damrath, U., and Gregoric, G.: Meso-gamma scale forecasts using the nonhydrostatic model LM, Meteorol. Atmos. Phys., 82, 75–96, 2003.
Stoelinga, M. T., Hobbs, P. V., Mass, C. F., Locatelli, J. D., Colle, B. A., Houze Jr., R. A., Rangno, A. L., Bond, N. A., Smull, B. F., Rasmussen, R. M., Thompson, G., and Colman, B. R.: Improvement of Microphysical Parameterization through Observational Verification Experiment (IMPROVE), B. Am. Meteorol. Soc., 84, 1807–1826, 2003.
Straka, J. M. and Anderson, J. R.: Numerical simulations of microburst-producing storms: some results from storms observed during COHMEX, J. Atmos. Sci., 50, 1329–1348, 1993.
Tong, M. and Xue, M.: Simultaneous estimation of microphysical parameters and atmospheric state with simulated radar data and ensemble square root Kalman filter, Part I: Sensitivity analysis and parameter identifiability, Mon. Weather Rev., 136, 1630–1648, 2008.
Thompson, G., Rasmussen, R. M., and Manning, K.: Explicit forecasts of winter precipitation using an improved bulk microphysics scheme, Part I: Description and sensitivity analysis, Mon. Weather Rev., 119, 734–754, 2004.
Thompson, G., Hall, B., Field, P., and Rasmussen, R.: A New Bulk Microphysical Parameterization in WRF, 7th WRF User's Workshop, Boulder CO, 2006.
Troen, I. B. and Mahrt, L.: A simple model of the atmospheric boundary layer; sensitivity to surface evaporation, Bound.-Lay. Meteorol., 37, 129–148, 1986.
Zrnić, D. S., Ryzhkov, A. V., Straka, J., Liu, Y., and Vivekanandan, J.: Testing a procedure for automatic classification of hydrometeor types, J. Atmos. Ocean. Tech., 18, 892–913, 2001.
Xue, M. et al.: The Advanced Regional Prediction System (ARPS) – a multiscale nonhydrostatic atmospheric simulation and prediction tool, Part II: Model physics and applications, Meteorol. Atmos. Phys., 76, 134–165, 2001.
Van den Heever, S. C. and Cotton, W. R.: The impact of hail size on simulated supercell storms, J. Atmos. Sci., 61, 1596–1609, 2004.

ACPD
10, 20461–20514, 2010

Table 1. Most important differences between COSMO-LAMI and MM5.

COSMO-LAMI	MM5V3
One way nesting	Two way nesting
3 domains up to 1km resolution	4 domains up to 1km resolution
50 eta levels	33 sigma levels
2.5 order local closure scheme for PBL	1 order non local closure scheme for PBL
N_0^g fixed	N_0^g predicted

ACPD
10, 20461–20514, 2010

Table 2. Numerical values of the microphysical parameters adopted for each sensitivity experiment.

Exp	ρ_g (10^6 g/m^3)	N_0^g (m^{-4})	a_g^0 (m(1−b) s^{-1})	b	c (kg m(−e))	e
1	0.2	4×10^4	442	0.89	169.6	3.1
2	0.2	4×10^5	442	0.89	169.6	3.1
3	0.2	4×10^6	442	0.89	169.6	3.1
4	0.4	4×10^4	93.35	0.50	209.44	3.0
5	0.4	4×10^5	93.35	0.50	209.44	3.0
6	0.4	4×10^6	93.35	0.50	209.44	3.0
7	0.9	4×10^4	140.03	0.50	471.24	3.0
8	0.9	4×10^5	140.03	0.50	471.24	3.0
9	0.9	4×10^6	140.03	0.50	471.24	3.0
10	0.9	4×10^6	193.2	0.37	471.24	3.0

ACPD
10, 20461–20514, 2010

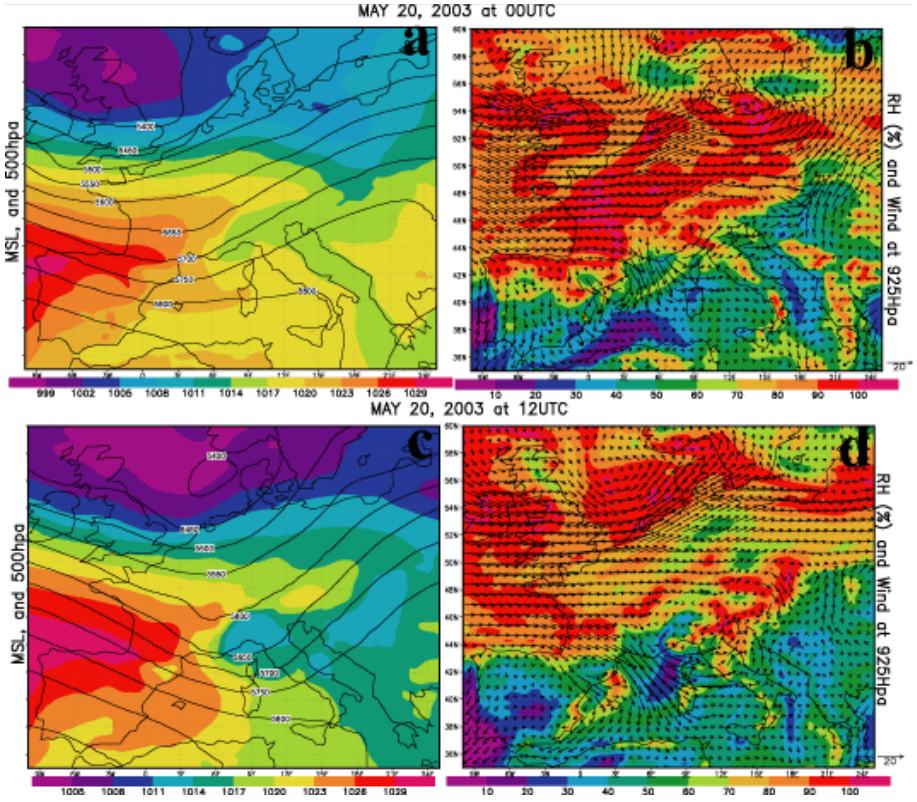

Fig. 1. Ecmwf analyses for mean sea level pressure (shaded colors, left panels **a** and **c**) and geopotential height at 500 hPa (black contours line, left panels a and c) and relative humidity (shaded colors, right panels **b** and **d**) and horizontal wind (wind vectors, right panels b and d) at 925 hPa. For 20 May 2003 at 00:00 UTC (upper panels), 12:00 UTC (lower panel).

ACPD
10, 20461–20514, 2010

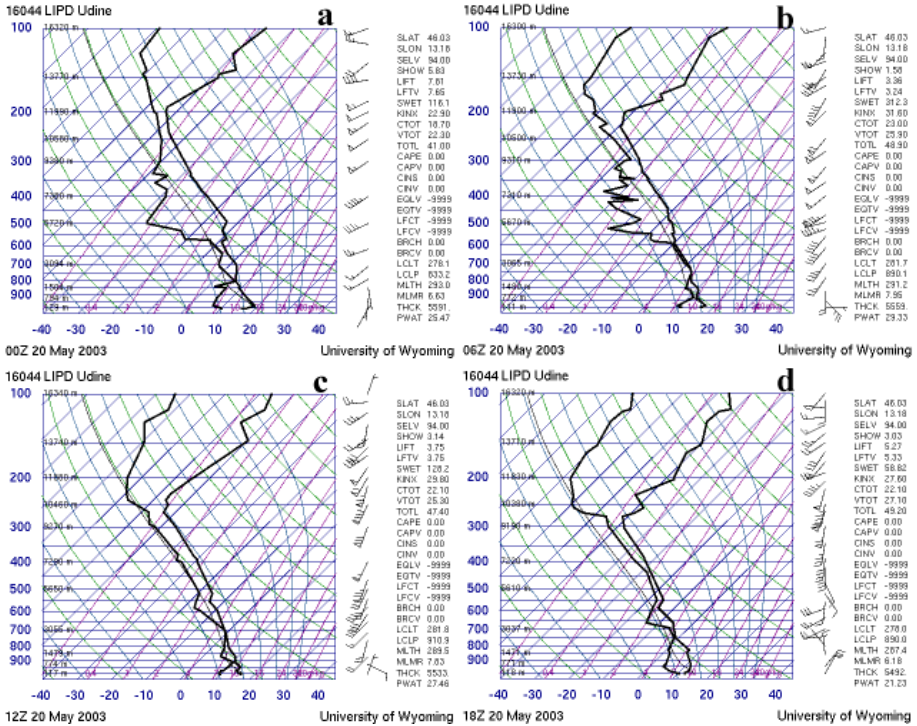

Fig. 2. Udine soundings for 20 May at: **(a)** 00:00 UTC; **(b)** 06:00 UTC; **(c)** 12:00 UTC; **(d)** 18:00 UTC.

ACPD
10, 20461–20514, 2010

Investigating the sensitivity of high-resolution mesoscale models

R. Ferretti et al.

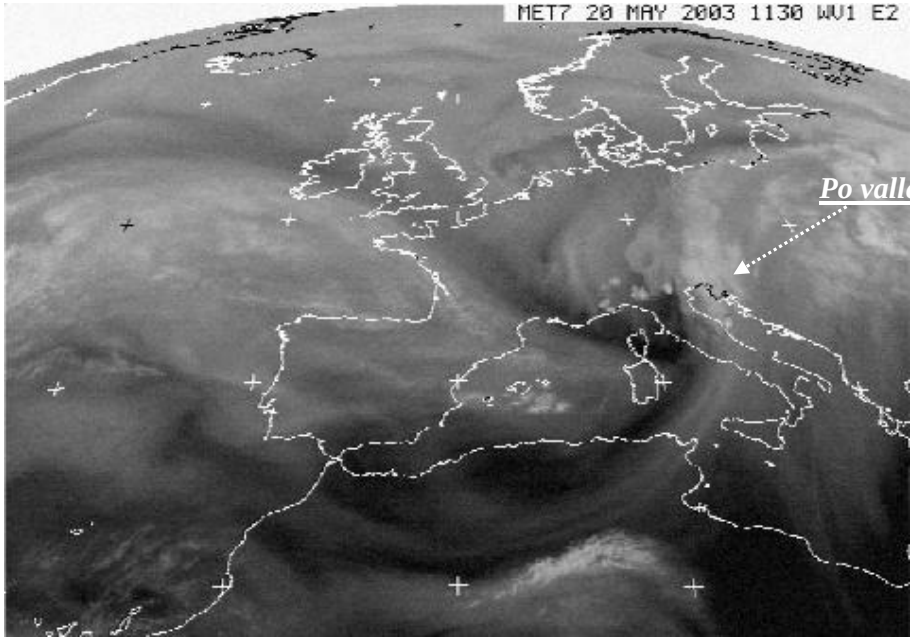

Fig. 3. Water vapor Meteosat imagery at 11:30 UTC 20 May. The dark area in the western Po Valley is the intrusion of cold dry air.

ACPD
10, 20461–20514, 2010

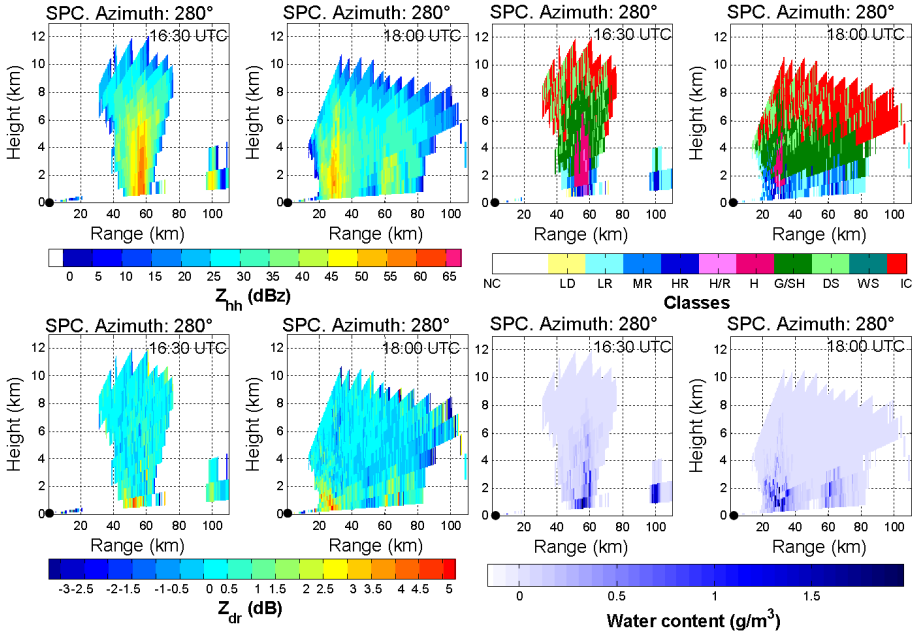

Fig. 4. RHIs at azimuth of 280° of hydrometeor classes (upper right panels) and water content (lower right panels) at 16:30 UTC (left panels) and 18:00 UTC (right panels) for SPC radar. On the left panels: RHI of Z_{hh} (upper panels) and Z_{dr} (lower panels) at 16:30 UTC (left panels) and 18:00 UTC (right panels) for SPC radar. The radar position is indicated with a black circle in the lower left corner of each subplot.

ACPD
10, 20461–20514, 2010

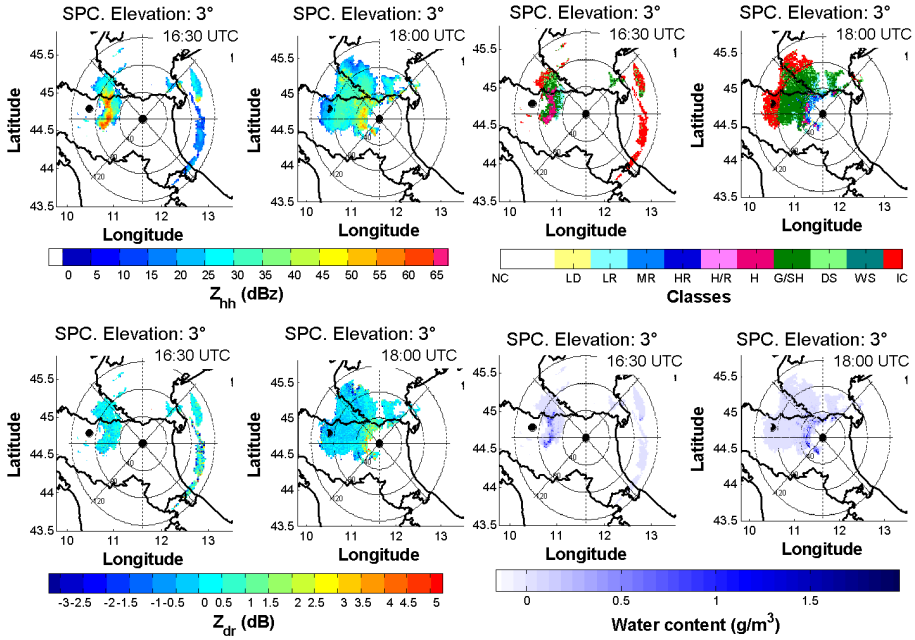

Fig. 5. As in Fig. 4 but for PPI scans at elevation angle of 3°.

ACPD
10, 20461–20514, 2010

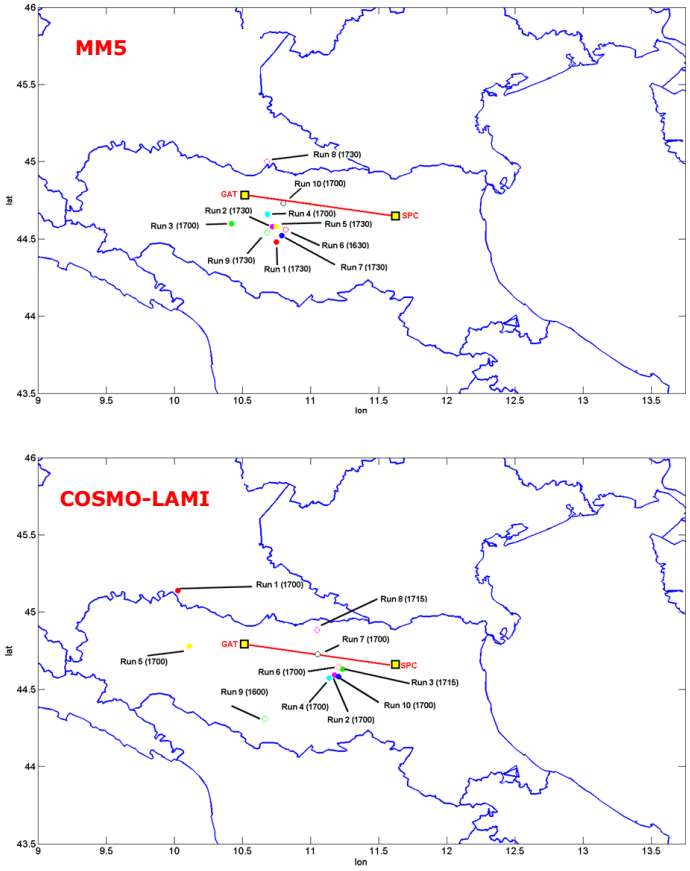

Fig. 6. Horizontal distribution of the cell for each sensitivity experiments for MM5 (top panel) and COSMO-LAMI (bottom panel). Next to each run, the reference time (UTC) is reported as well. The red line connecting the two radars is indicating the cross-section.

ACPD
10, 20461–20514, 2010

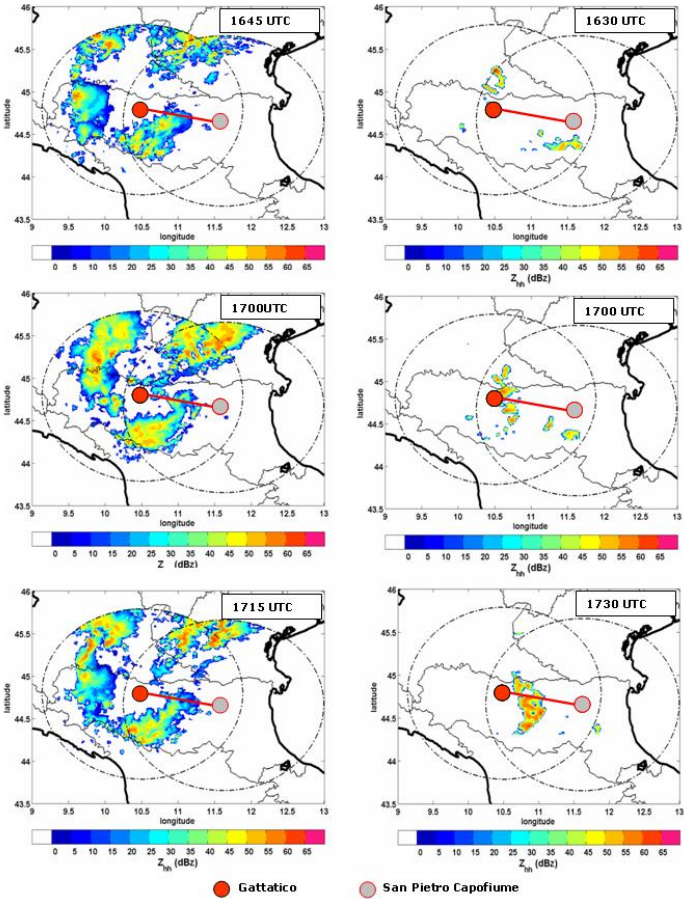

Fig. 7. 2-D maps of reflectivity within the radar coverage area between 16:45 and 17:15 UTC for COSMO-LAMI setting 7 (left) and between 16:30 and 17:30 UTC for MM5 setting 10 (right).

ACPD
10, 20461–20514, 2010

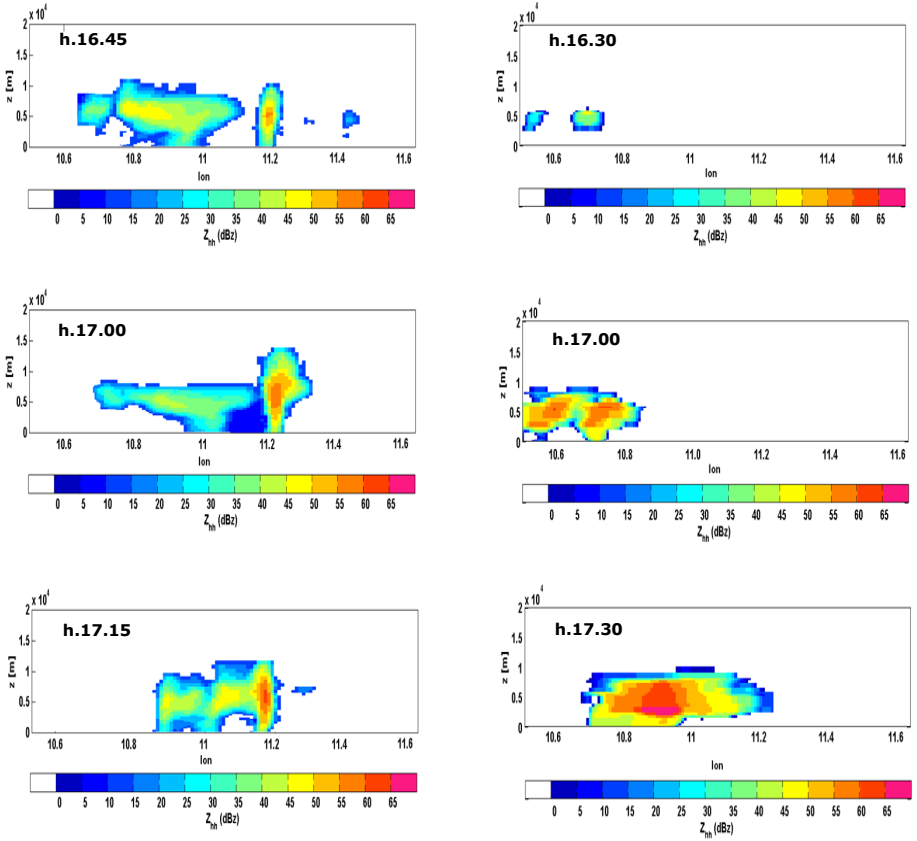

Fig. 8. Vertical cross-sections (taken along the red line in Fig. 6) of reflectivity from 16:45 to 17:15 UTC for COSMO-LAMI (left column) and from 16:30 to 17:30 UTC for MM5 (right column) for the azimuth of 280° from the north direction.

ACPD
10, 20461–20514, 2010

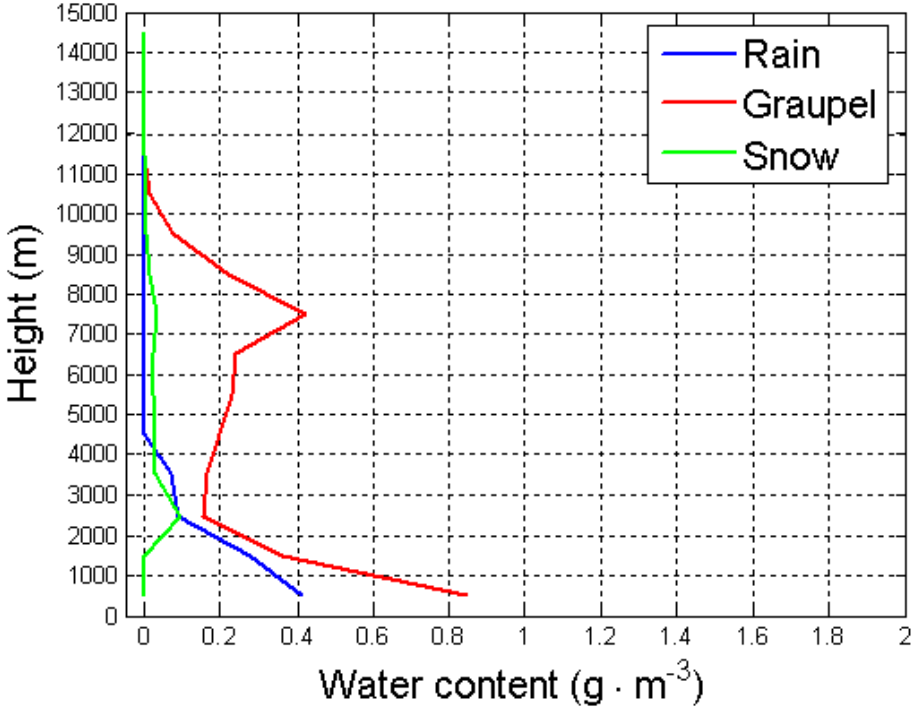

Fig. 9. Mean observed vertical profiles of water content for the three species of hydrometeors: Rain, Graupel and snow on a grid box of $20\times20\times10\,km^3$ centered on the convective cell showed on Fig. 4 (right).

ACPD
10, 20461–20514, 2010

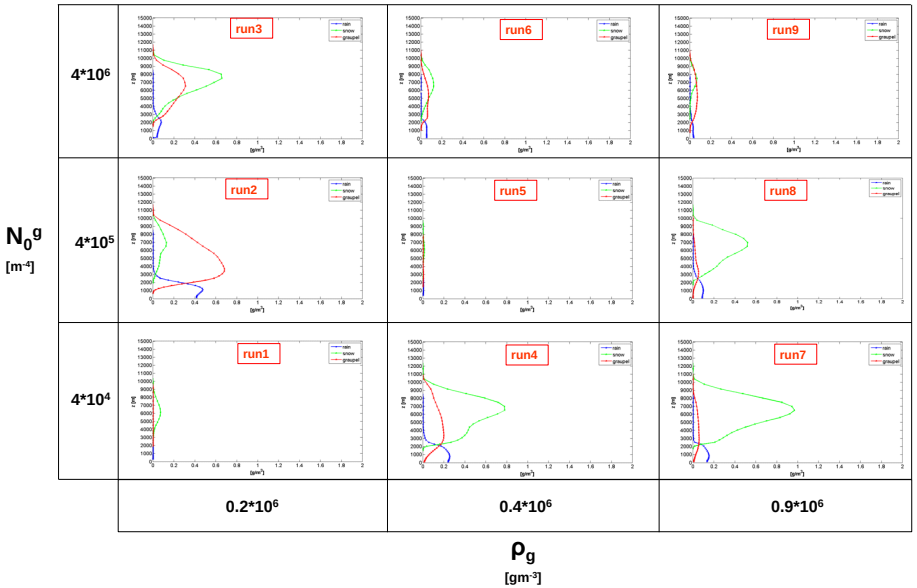

Fig. 10a. COSMO-LAMI Mean vertical profiles of water content for the three species of hydrometeors: rain, graupel and snow on a grid box of $20\times20\times10\,km^3$ centered on each convective cell showed on Fig. 6.

ACPD
10, 20461–20514, 2010

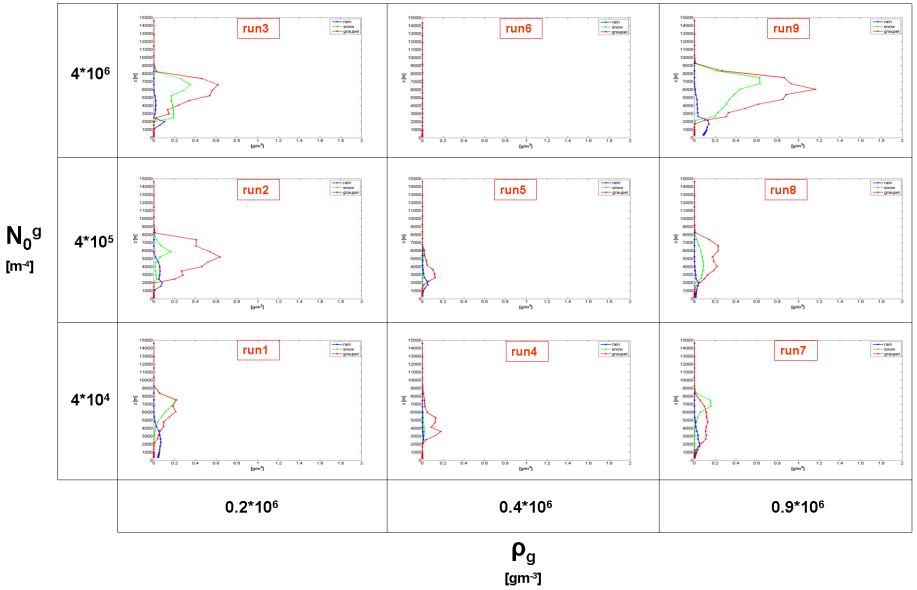

Fig. 10b. As for **(a)** but for MM5.

ACPD
10, 20461–20514, 2010

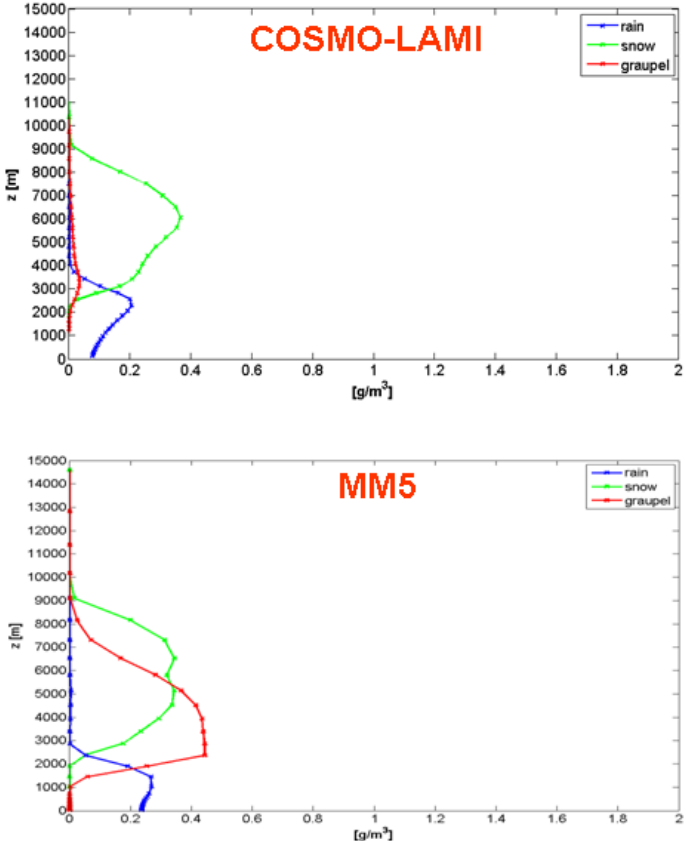

Fig. 10c. As for **(a)** but for setting 10 for COSMO-LAMI and MM5.

ACPD
10, 20461–20514, 2010

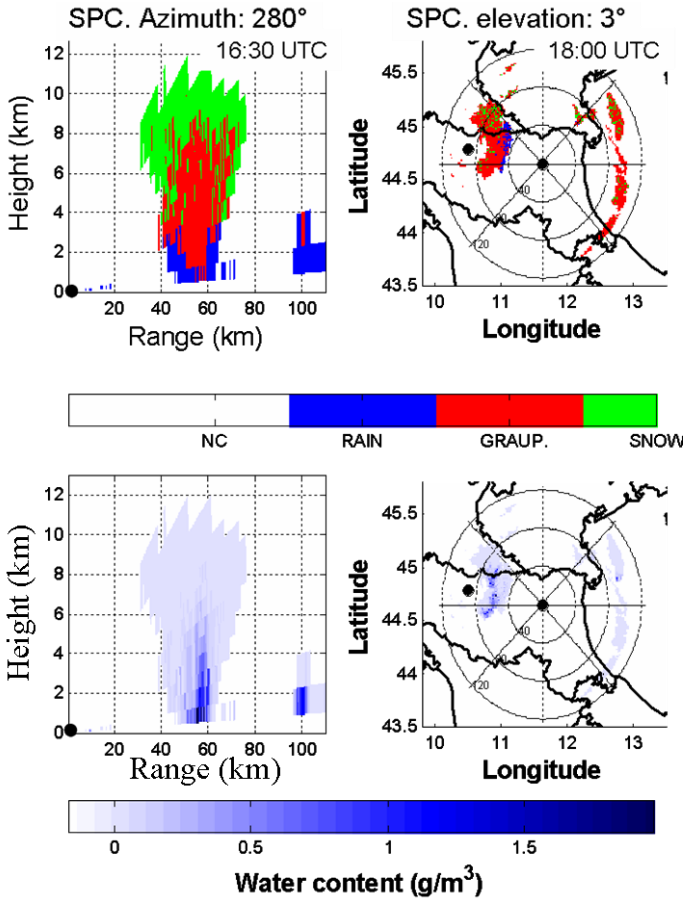

Fig. 11. RHIs at azimuth of 280° of hydrometeor classes (upper left panel) and water content (lower left panel) at 16:30 UTC for SPC radar. PPI scans at elevation angle of 3° of hydrometeor classes (upper right panels) and water content (lower right panels) at 16:30 UTC. The radar products are reduced to three categories: snow (green), graupel (red) and rain (blue).

ACPD
10, 20461–20514, 2010

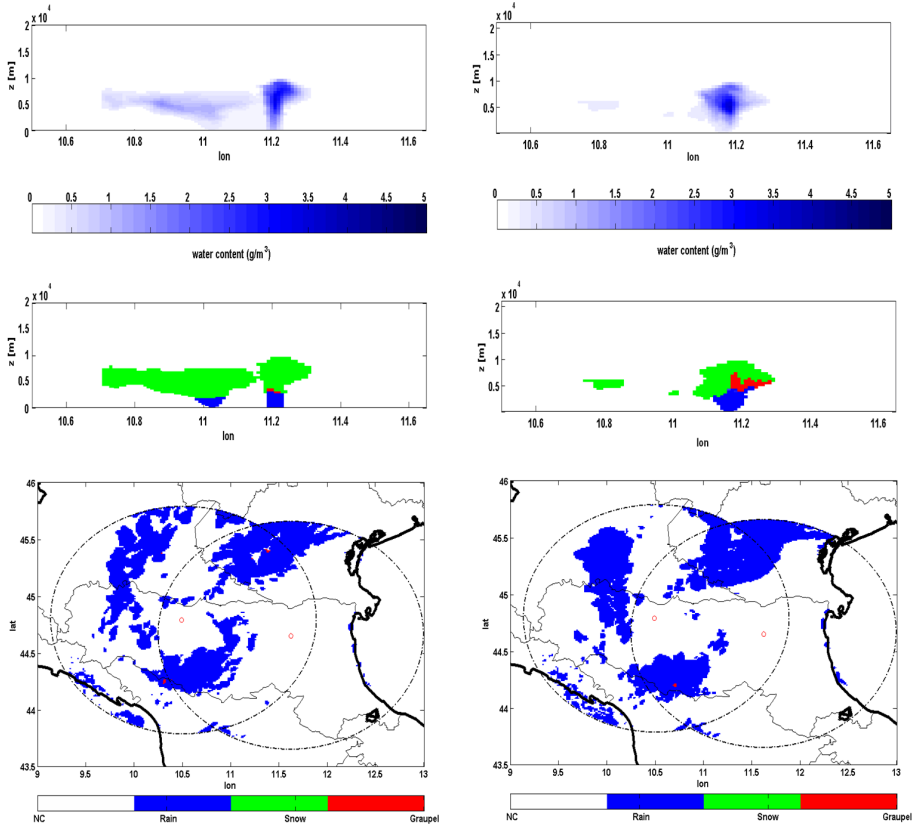

Fig. 12. Vertical cross-sections (taken along the red line in Fig. 6) of water content (upper panel) and hydrometeor classes (middle panel); 2-D maps of hydrometeor classes (lower panel) as in Fig. 7 (middle left panel). Setting 7 at 17:00 UTC (left side) and setting 2 at 17:15 UTC (right side) for COSMO-LAMI.

ACPD
10, 20461–20514, 2010

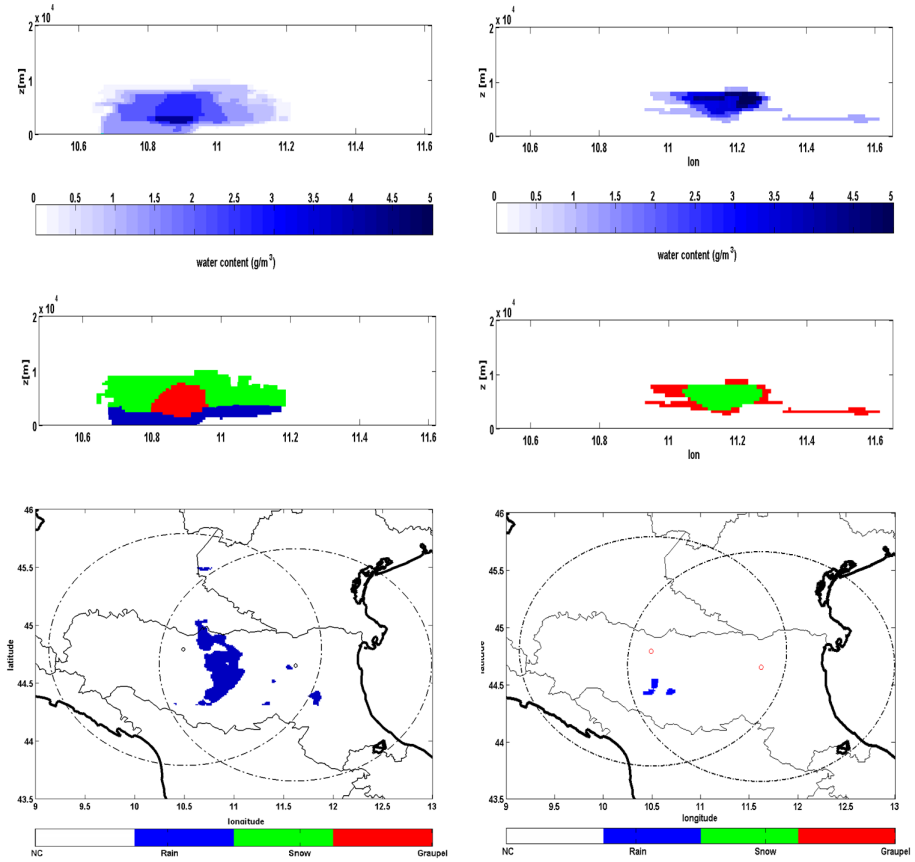

Fig. 13. As for Fig. 12 but for MM5 setting 10 at 17:30 UTC (left side) and setting 3 at 17:00 UTC (right side).

ACPD
10, 20461–20514, 2010

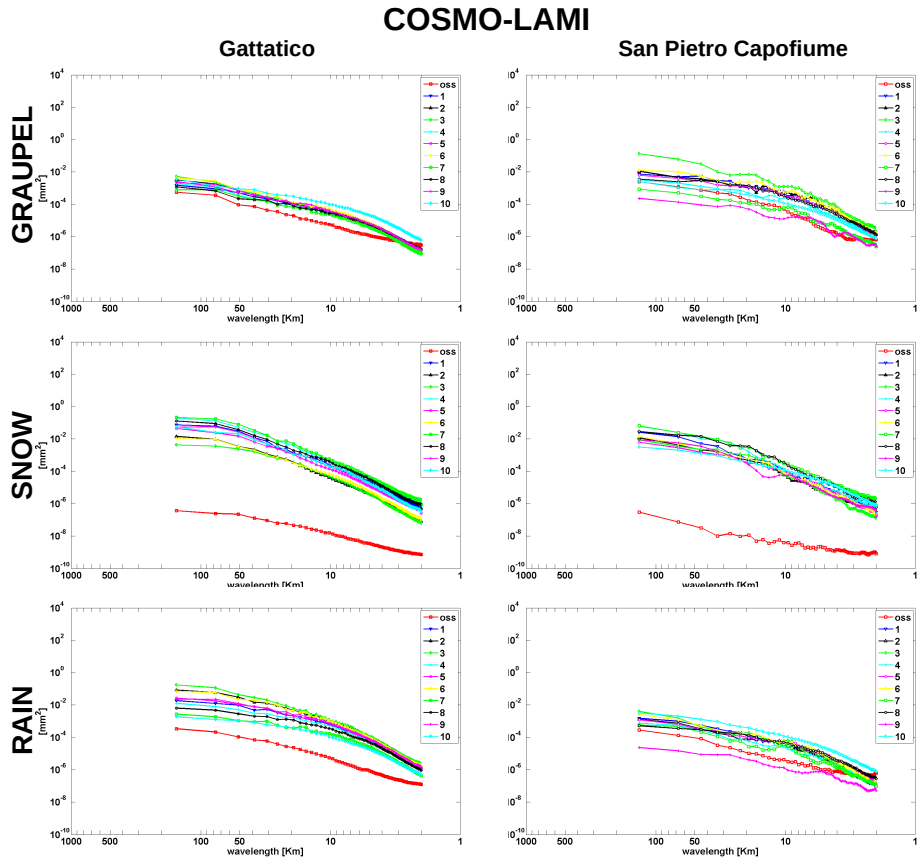

Fig. 14a. Mean spectra for all experiments for COSMO-LAMI at Gattatico (left column) and San Pietro Capofiume (right column) for: hail (first row); snow (second row); rain (third row).

ACPD
10, 20461–20514, 2010

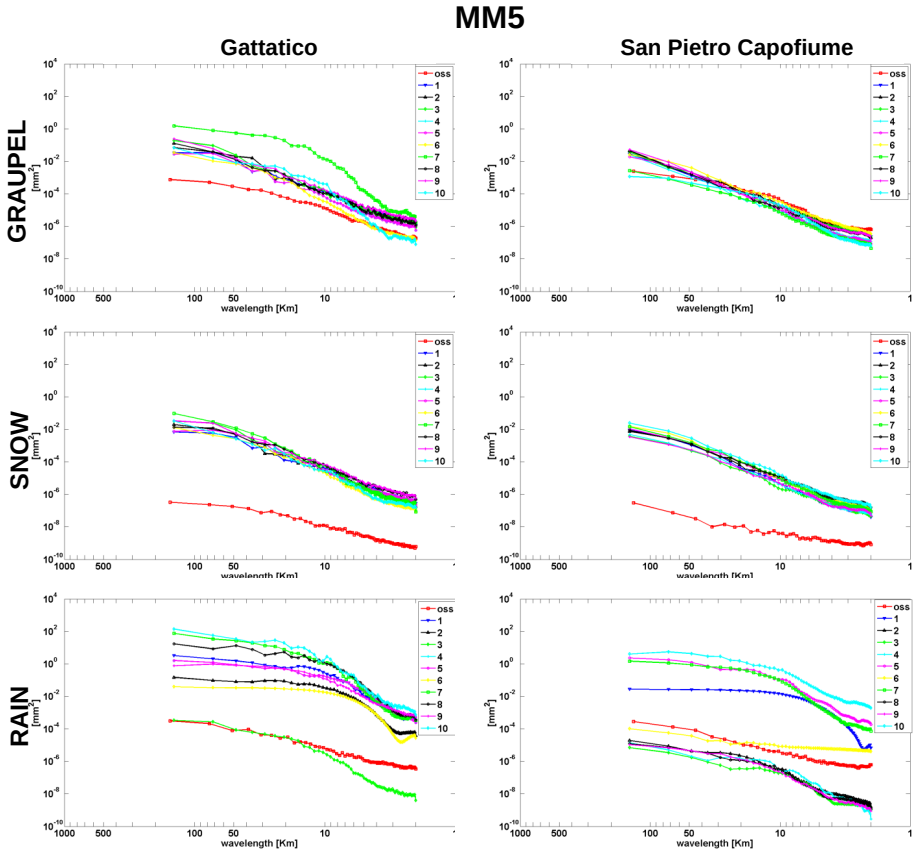

Fig. 14b. As for Fig. 14a but for MM5 experiments.

ACPD
10, 20461–20514, 2010